1993AJ....105.1251W

THE ASTRONOMICAL JOURNAL VOLUME 105, NUMBER 4 APRIL 1993

A SURVEY OF THE PISCES–PERSEUS SUPERCLUSTER. V. THE DECLINATION STRIP +33.5° TO +39.5° AND THE MAIN SUPERCLUSTER RIDGE

GARY WEGNER
Department of Physics and Astronomy, Dartmouth College, Hanover, New Hampshire 03755

MARTHA P. HAYNES AND RICCARDO GIOVANELLI
National Astronomy and Ionosphere Center[1] and Department of Astronomy, Cornell University, Ithaca, New York 14853
Received 1992 October 14; revised 1992 November 18

ABSTRACT

Measurements of 544 radial velocities, 229 optical and 315 in the 21 cm H I line, are presented for galaxies, mostly in the declination strip $+33.5° < \delta < +39.5°$ in the region of the Pisces–Perseus supercluster. These are combined with other available data to investigate the linear structure identified as the main supercluster ridge. The main ridge of the supercluster extends at least $50h^{-1}$ Mpc before it disappears into the zone of avoidance east of Perseus. Confinement both on the plane of the sky and in the velocity dimension imply an axial ratio of greater than ten to one and an inclination with respect to the plane of the sky of less than about 12 degrees. The smoothed volume density contrast over the whole ridge averages more than a factor of 6 relative to the average density derived for the whole sample. The relative proximity, low inclination to the plane of the sky, and high contrast relative to the foreground and background, help to make the Pisces–Perseus filament one of the most prominent features in the extragalactic sky on large scales.

1. INTRODUCTION

The study of the large-scale distribution of galaxies in the local universe has been a major topic of research in the last decade. In particular, advances in the capabilities of detectors and spectrometers at both optical and radio wavelengths have contributed to tremendously increase the number of measured galaxy redshifts and thus have led to a great improvement in our ability to judge the topology of the galaxy distribution. Although the existence of large deviations from the isotropic expansion predicted by Hubble's law has also been confirmed in this period, the application of the simple redshift–distance relation to major redshift surveys allows us a fair approximation to the picture of the distribution of luminous matter in the nearby universe. It is now clear that the structure on large scales is complex. While it is quite easy to identify the galaxy to which any star chosen at random in the universe belongs, it is much more difficult to find the hierarchy in which a random galaxy exists.

Among the primary aims of attempts to detail the three-dimensional structure in the local universe are the mapping of individual superclusters, the determination of their scale parameters and the characterization of their morphology. We require not only qualitative descriptions of the distribution of galaxies in a three-dimensional sense, but also quantitative measures of the topology that can be used to test models for the formation and evolution of such structures. Indeed, all of these objectives are the goals of ongoing studies by a number of groups and much progress has been made in recent years. The identification of individual supergalactic objects is new territory in astronomy, not without its controversies and limitations, the latter imposed more by our inadequate observational samples than by our imaginations.

The sky distribution of galaxies in the local universe is illustrated in Fig. 2 of Giovanelli & Haynes (1991). Its inspection promptly reveals that the three most prominent large-scale features are: (1) the zone of avoidance, (2) the Virgo cluster and the supergalactic plane, and (3) the main ridge of the Pisces–Perseus (PP) supercluster, which runs southwestward from the Perseus cluster at (R.A.,Dec.) $\simeq (3.2^h, +42°)$. It is important to recognize the differences in the distances of these objects. The zone of avoidance arises locally from the structure of the Milky Way; the relatively nearby Virgo cluster has a radial velocity of 1050 km s^{-1}, while that of the Perseus cluster is 5500 km s^{-1}, which places it five times farther than Virgo, if we neglect deviations from Hubble flow. The difference in distance implies that apparent magnitude-limited surveys, of which typical redshift surveys are a fair approximation, sample 3.5 mag intrinsically fainter galaxies in Virgo than they do in PP. Nonetheless, PP represents a projected overdensity that rivals that of the Local Supercluster, and significantly exceeds the latter in linear size. How both our viewing aspect and the characteristics of the PP supercluster combine to make this prominent feature, is discussed in Sec. 4. Conversely, it should be noted that the structure discussed in this paper may not be representative of "typical" structures in the local universe: we chose PP as the focus of our observational effort precisely because of its prominence in the sky distribution of bright and large, nearby galaxies: hardly an unbiased choice. The PP supercluster was identified as an exceptional feature quite early by Bernheimer (1932). Seminal quantitative work was produced by Einasto *et al.* (1980) and Gregory *et al.*

[1]The National Astronomy and Ionosphere Center is operated by Cornell University under a management agreement with the National Science Foundation.

© American Astronomical Society • Provided by the NASA Astrophysics Data System

1993AJ....105.1251W

(1981), which outlined the major characteristics of the structure, in spite of the then meager redshift data base.

As evident also in Fig. 1 of Giovanelli *et al.* (1986: hereafter referred to as GHC), the main ridge of the supercluster extends across six hours of right ascension, roughly $22^h < \text{R.A.} < 4^h$. It extends westward from the Perseus cluster to the south where it becomes harder to trace in the region west of $\text{R.A.} = 0^h$. Although the supercluster can be traced throughout the region of our overall survey and possibly beyond (Haynes & Giovanelli 1988), the highest density regions outline a roughly continuous structure in the northern portions ($\text{Dec.} > +25°$). This high density volume is linear in structure, extending east to west across the survey area and is confined in the perpendicular sky direction and in redshift. We shall refer to this extragalactic object as the "Pisces–Perseus ridge" and it is the subject of the current paper.

In a series of earlier papers, we have presented the results of our H I survey of the Pisces–Perseus supercluster, generally covering separate zones of declination as they were completed or significantly updated (Giovanelli & Haynes 1985; Giovanelli *et al.* 1986; Haynes *et al.* 1988; Giovanelli & Haynes 1989). In the past, our observational efforts were limited to H I emission line spectra of the spiral galaxies. Because in the northern section of the region (which is particularly important because it includes the highest density supercluster ridge) morphological segregation induces a reduction in the proportional representation of late-type galaxies, and because of physical restrictions associated with the radio telescopes that have been used, we have undertaken to complement the radio line observations with optical spectroscopic ones, thus improving the completeness of the sample in high density regions of particular dynamical importance. The results of 574 optical and radio measurements of radial velocities of galaxies are included in Sec. 2. In Sec. 3, we investigate the structure of the main ridge in three dimensions, identifying clusters and groups dynamics. In the fourth section, the effects of the favorable viewing aspect and the proximity of the supercluster are examined to demonstrate how similar, but differently oriented structures could escape notice in galaxy surveys. The characteristics of the Pisces–Perseus ridge and our impressions of its relevance to general questions concerning large-scale topology are summarized in the conclusion.

2. RESULTS FOR THE REDSHIFT SAMPLE

Some of the highest density concentrations in the PP supercluster are found in the declination strip around +36°, including Abell 262 and portions of the NGC 383/NGC 508 cluster. At the same time that morphological segregation increases the proportional representation of early-type objects, the available radio telescopes impose their own limitations. At high zenith angles, the Arecibo 305 m telescope suffers from vignetting and spillover, which both decrease the system sensitivity quickly with increasing zenith angle. Simultaneously, tracking time shortens until the northern limit is reached at about +38°. Our alternative telescope of choice in the northern hemisphere was the late 91 m telescope at Green Bank, a smaller and more restricted transit instrument. Because of the much lower sensitivity and the need for morphological representation by high surface brightness observations, we have augmented the H I observations in this strip with optical spectroscopic redshift measurements. In this section, we report the results of both optical and radio surveys. While they refer principally to the declination strip 33.5° to 39.5° of PP, many redshifts correspond to galaxies in immediately adjacent regions.

2.1 Optical Data

Observations were made with the 2.4 m Hiltner telescope of the Michigan–Darthmouth–MIT (MDM) Observatory using the Mark III spectrograph. The Mark III is a high efficiency grism spectrograph with all glass transmission optics designed by W. A. Hiltner and built at the University of Michigan. For the present observations, a 300 lines/mm grism was used with either a Thompson or a RCA CCD as the detector. With an entrance slit of 1.9 arcsec width, this setup yields resolutions of 11 and 13 Å, respectively with an approximate spectral coverage of 4000 to 7200 Å. All data reductions were done at Dartmouth using the IRAF software package (Tody 1986); in particular, the standard longslit routines were used to flatten, subtract the background, and extract wavelength corrected one-dimensional spectra. Velocities were obtained from the absorption spectra of the galaxies using nightly K giant standard star spectra and a Fourier coefficient program (JKFOUR) similar to that described by Sargent *et al.* (1977) and kindly supplied by Roger Davies. Emission line spectra were measured using the "deblending" option in the "splot" IRAF routine.

Table 1 contains the optical redshift measurements of 213 galaxies observed with the Hiltner telescope. Sample objects were selected, for which, at the time of the observations, no optical redshifts were available to us. The entries include:

Column (1)—Identification in the *Catalog of Galaxies and Clusters of Galaxies* (Zwicky *et al.* 1961-68: hereafter referred to as CGCG), that is, the field number and then the entry number within that field.

Column (2)—*Uppsala General Catalog* (UGC) entry number (Nilson 1973).

Column (3)—*New General Catalogue* (NGC) or IC number or alternate name.

Columns (4) and (5)—1950 Right Ascension (R.A.) and 1950 Declination (Dec). For galaxies brighter than $m = 14.5$, positions were obtained from Dressel & Condon (1976). For others, coordinates were obtained from the CGCG or, when higher accuracy than that of the CGCG is manifest, they were obtained from the Palomar Sky Survey (PSS) prints using a standard overlay program, with an estimated accuracy of 10″.

Column (6)—Morphological type code index based on the simple scheme: 0—Elliptical, 1—S0, 3—Sa, 5—Sb, 7—Sc, 9—Irregular, 10—Peculiar, with intermediate types allowed. A "B" indicates the presence of a bar. This coding

© American Astronomical Society • Provided by the NASA Astrophysics Data System

1993AJ....105.1251W

is based on the Hubble typing scheme employed by Nilson in the UGC. Types have been estimated by eye examination of the PSS prints. Morphological types of Nilson, when available, have been given priority, except in the few cases where a re-examination of the morphology was warranted (e.g., the classification of a spiral in a system classified as "multiple" by Nilson, etc.); consistency with Nilson's classification scheme was maintained inasmuch as possible, for non-UGC galaxies.

Column (7)—Major and minor diameters in arcmin from the UGC where available or else measured by eye from the PSS prints.

Column (8)—Inclination in degrees derived from the axial ratio following Haynes & Giovanelli (1984: hereafter referred to as HG84).

Column (9)—Magnitude given in the CGCG or the UGC.

Column (10)—Corrected magnitude m_c, after applying corrections for galactic and internal extinction, redshift and systematic effects as discussed by HG84.

TABLE 1. Galaxies with new optical redshifts.

CGCG	UGC	NGC/IC	RA	Dec	T	a x b	i	m_z	m_c	V_{sun}	σ	e/a	V_o	log L
518-012	62	N 5	000512.0	+350500	0	1.20 x 0.70		14.60	14.09	5111	41	a	5358	9.97
499-073			000912.0	+325000	5	0.45 x 0.20	66	15.40	14.59	14034	58	a	14275	10.62
499-084			001136.0	+281600	1	0.55 x 0.50	25	15.30	14.94	7113	46	a	7343	9.90
499-085			001148.0	+281400	1	0.40 x 0.30	43	15.50	15.10	7134	52	a	7364	9.84
478-047	146		001306.0	+271000	1	1.20 x 0.60	62	15.40	15.08	7400	54	a	7626	9.88
499-092			001349.0	+300540	1	0.60 x 0.20	75	14.80	14.16	6329	48	a	6562	10.12
500-013			002106.0	+301700	1	0.80 x 0.50	52	15.10	14.64	6248	49	a	6477	9.92
519-008		I1550	002148.6	+375431	1	0.80 x 0.80	0	15.10	14.60	5818	42	a	6058	9.79
519-009			002724.1	+380306	5	0.40 x 0.40	0	15.50	15.04	11112	60	e	11353	10.24
500-044	332	N 149	003112.0	+302700	1	1.30 x 0.80	53	15.00	14.59	4712	70	a	4936	9.70
500-054	381		003530.0	+303700	5	1.60 x 1.20	43	15.30	14.88	5447	56	a	5669	9.70
500-062	395		003613.5	+311607	5	1.20 x 0.70	55	15.40	14.89	791	200	a	1014	8.20
500-066	431		003800.0	+295300	5	1.20 x 1.00	35	15.10	14.70	5195	63	a	5413	9.73
500-074			004007.5	+293850	0	0.65 x 0.45		14.70	14.26	4896	41	a	5113	9.86
500-080			004124.0	+300500	1	0.60 x 0.40	49	15.10	14.67	5481	48	a	5698	9.79
500-081			004303.7	+293343	1	0.40 x 0.25	52	14.70	14.18	5083	44	e	5298	9.92
500-088			004406.0	+274017	1	0.60 x 0.30	62	15.40	14.96	6933	60	e	7142	9.87
501-016			004512.0	+294100	1	0.50 x 0.50	0	15.40	15.08	4995	60	e	5209	9.55
501-017			004524.0	+294100	1	0.50 x 0.50	0	15.60	15.19	10498	32	a	10711	10.13
501-018			004530.0	+282000	1	0.60 x 0.25	68	15.00	14.46	7045	34	a	7255	10.08
501-026			004824.5	+291553	1	0.70 x 0.70	0	15.50	15.18	5102	60	e	5313	9.53
501-030		N 282	005000.0	+302207	0	0.80 x 0.70		14.70	14.23	6542	55	a	6754	10.12
501-033		N 287	005045.3	+321243	2	0.70 x 0.50	45	14.80	14.28	5556	44	a	5772	9.96
501-034			005052.5	+310853	1	0.80 x 0.60	43	15.50	15.10	5456	44	a	5669	9.61
501-039	555		005206.0	+283607	2	1.00 x 0.20	90	14.90	14.23	6783	42	a	6990	10.15
501-046	567		005236.0	+312800	1	1.10 x 0.40	72	14.90	14.31	6072	39	a	6285	10.02
501-054		N 318	005518.0	+300900	1	0.50 x 0.20	69	15.20	14.70	5222	50	a	5429	9.75
501-067			005906.0	+295300	1	0.60 x 0.45	43	15.00	14.55	6587	45	a	6792	9.99
501-070			005924.5	+321107	1	0.50 x 0.40	38	15.10	14.69	4190	54	a	4401	9.56
501-095		N 394	010542.0	+325300	1	0.55 x 0.30	58	14.80	14.25	4310	50	a	4518	9.76
520-017	703	N 389	010540.1	+392540	2	1.40 x 0.40	79	15.00	14.41	5219	55	a	5437	9.86
520-018	707	N 393	010547.2	+392236	0	1.70 x 1.40		13.30	12.85	6014	42	a	6236	10.60
501-100		N 398	010606.0	+321500	1	0.70 x 0.30	67	15.40	14.90	4859	86	a	5066	9.60
501-102			010630.0	+314200	1	0.60 x 0.40	49	15.30	14.88	5099	58	a	5304	9.65
501-114			010736.0	+320700	1	0.70 x 0.15	90	15.50	14.88	5319	66	a	5524	9.68
501-117			010805.5	+321940	2B	0.55 x 0.40	44	15.40	14.98	5615	25	a	5820	9.69
501-120			010824.0	+322600	2	0.60 x 0.40	49	15.30	14.87	4889	59	a	5095	9.61
501-125		I1636	010848.0	+330600	1	0.40 x 0.25	52	14.90	14.45	5632	51	a	5839	9.88
501-128			010922.8	+314423	5	0.40 x 0.30	43	15.30	14.84	5208	60	e	5411	9.68
501-129		I1638	010935.5	+330547	0	0.65 x 0.65		14.90	14.45	4649	50	a	4855	9.85
520-024			011000.1	+364531	1	0.80 x 0.35	66	15.30	14.65	9615	64	a	9829	10.27
502-014			011303.0	+313347	2	0.80 x 0.50	50	15.40	14.85	4496	60	e	4700	9.57
502-017	812	I1659	011319.8	+300509	0	1.60 x 1.10		14.60	14.20	6842	34	a	7027	9.95
502-029		I 92	011700.0	+323007	2	0.75 x 0.45	54	15.10	14.61	5172	60	e	5355	9.78
502-033	862		011724.5	+331439	0	0.90 x 0.90		14.50	14.13	5071	85	a	5255	9.97
502-034	870	N 472	011740.4	+322655	5	1.30 x 1.10	33	14.20	13.72	5275	41	x	5471	10.14
502-038		I1673	011800.0	+324800	0	0.45 x 0.45		14.60	14.09	5102	50	a	5302	9.96
521-004	878		011813.9	+333812	1	1.20 x 0.90	43	14.70	14.26	4043	63	a	4245	9.70
502-043			011818.0	+330800	0	0.60 x 0.60		14.90	14.45	5186	75	a	5387	9.83
502-044			011824.0	+325000	0	0.45 x 0.45		15.00	14.58	5018	95	a	5218	9.75
502-047			011849.0	+332033	2	0.80 x 0.50	52	15.50	14.78	21490	25	a	21691	10.91
502-046	901		011849.1	+322041	5	0.70 x 0.20	79	14.50	13.44	4748	41	a	4947	10.16
502-049		I1680	011858.0	+330127	2	0.60 x 0.60	0	14.90	14.46	4377	33	a	4577	9.68
521-011			011959.4	+334227	2	0.65 x 0.22	74	15.50	14.93	5381	60	e	5582	9.67
521-012			0120 1.5	+385945	2	0.60 x 0.30	62	14.60	13.81	7779	42	a	7992	10.43
502-069			0121 0.0	+322500	1	0.60 x 0.40	49	14.70	14.04	12221	61	a	12418	10.72
502-092	1058	N 566	012612.0	+320500	1	1.50 x 0.35	85	14.60	13.95	5460	49	a	5653	10.07
521-052			013238.8	+352450	2	0.90 x 0.25	80	15.50	14.86	5080	65	a	5277	9.65
521-053			013245.8	+351244	1	0.70 x 0.40	56	15.20	14.67	5132	60	e	5328	9.73
521-059	1161		013519.8	+362118	5	1.00 x 0.90	27	15.00	14.68	5213	73	a	5410	9.74
503-009			014042.0	+302100	2	0.70 x 0.30	67	15.50	14.94	9765	66	a	9944	10.17
503-013	1213		014118.0	+310433	1	1.00 x 0.90	27	14.90	14.50	10421	50	a	10601	10.40
521-077			014227.5	+340044	5	0.70 x 0.30	67	15.20	14.39	5423	44	a	5610	9.89
503-029			014742.0	+324800	1	0.50 x 0.20	69	15.40	14.78	9982	39	a	10162	10.25
522-023	1316		014823.7	+343729	5	1.40 x 0.80	56	16.50	16.07	5123	53	a	5308	9.17
503-037			014840.3	+325813	2	0.90 x 0.90	0	15.30	14.83	10199	42	a	10379	10.25
503-038			014842.0	+331500	1	0.30 x 0.30	0	15.50	15.00	11231	60	e	11412	10.26
503-041	1327		0149 0.0	+301800	0	1.40 x 0.70		14.90	14.65	4560	49	a	4733	9.64
522-030			014920.6	+354724	1	0.55 x 0.30	58	15.50	14.96	4595	54	a	4782	9.52
522-032	1339		014928.7	+353535	1B	1.20 x 1.10	24	15.00	14.65	4063	44	a	4249	9.54
522-039	1348	N 708	014954.0	+355500	0	3.00 x 2.50		14.80	14.36	4898	45	a	5085	9.82
522-053			015059.9	+362342	2	0.55 x 0.40	44	15.40	14.89	4430	52	a	4617	9.52
522-054			015114.8	+354018	2	0.55 x 0.20	72	15.20	14.58	4293	60	e	4478	9.62
522-057			015155.6	+371701	2B	0.70 x 0.50	45	15.40	14.86	4615	99	a	4804	9.57
522-072			015324.8	+351943	5	0.40 x 0.30	43	15.20	14.64	5338	60	e	5521	9.78
503-057		N 738	015354.0	+324900	1	0.25 x 0.25	0	15.50	15.12	4219	34	a	4395	9.39
503-059			015400.0	+330113	2	0.80 x 0.60	43	14.80	14.27	4374	38	a	4551	9.76
522-084	1434		015441.5	+360041	2	1.50 x 0.50	75	15.40	14.85	4564	63	a	4748	9.56
503-068			015721.0	+314907	1	0.80 x 0.30	71	15.40	14.85	5121	98	a	5292	9.66
503-069	1480	N 778	015725.6	+310419	1	1.10 x 0.50	65	14.20	13.66	5420	58	a	5589	10.18
503-072	1488	N 780	015742.0	+275900	5	1.80 x 1.00	58	14.60	13.91	5260	67	a	5420	10.05
522-104			015759.4	+383236	1	0.55 x 0.30	58	15.20	14.55	5614	60	e	5802	9.85
503-076	1509	N 785	015846.1	+313506	0	1.50 x 0.90		13.90	13.49	4952	36	a	5121	10.17
482-055			015948.0	+272013	2	1.00 x 0.25	83	15.00	14.39	4885	44	a	5041	9.80
503-078	1539	N 798	020024.0	+315000	0	1.20 x 0.50		14.70	14.25	4947	50	a	5116	9.86
503-079	1557	N 804	020106.0	+303500	1	1.40 x 0.25	90	14.70	14.00	5268	43	a	5433	10.02
504-004	1566	N 805	020137.5	+283420	1B	1.10 x 0.70	51	14.70	14.22	4600	49	a	4759	9.81
504-011	1596		020336.0	+294500	1	1.30 x 0.90	47	14.80	14.38	4776	59	a	4937	9.78
522-113	1604		020417.7	+365133	1	1.50 x 0.90	54	15.00	14.63	5290	48	a	5469	9.77
504-016		N 816	020515.6	+290111	12	0.40 x 0.40	0	15.30	14.87	11104	60	e	11266	10.30
504-021			020700.0	+291700	1	0.70 x 0.25	73	15.50	14.97	4997	54	a	5154	9.58
504-022			020742.0	+310600	0	0.65 x 0.40		15.00	14.56	5062	45	a	5224	9.76
522-134	1691		020910.2	+390006	1	1.80 x 1.60	28	14.60	14.11	5528	47	a	5710	10.02
522-135	1695	N 845	020918.2	+371433	5	1.80 x 0.50	80	14.50	13.45	4359	60	a	4536	10.08
522-139			021108.5	+352911	1	0.60 x 0.60	0	15.50	14.94	10995	42	a	11166	10.27
504-037		N 860	021204.7	+303246	0	0.50 x 0.40		15.10	14.60	8817	50	e	8992	10.21
523-004	1735		021238.3	+351729	0	1.40 x 1.10		14.00	13.47	8044	40	a	8214	10.59
504-051			021516.5	+324417	5	0.70 x 0.25	73	15.40	14.47	8782	60	e	8943	10.26
523-016			021539.0	+365404	1	0.65 x 0.20	77	15.50	14.75	7749	42	a	7921	10.05
523-018	1781	I1792	021601.6	+341358	5	1.60 x 1.50	21	15.00	14.56	10434	51	a	10598	10.37
504-060	1805		021801.1	+323643	5	1.00 x 0.22	90	14.50	13.29	5399	35	a	5558	10.32
504-077	1889		022306.0	+295700	1B	1.20 x 1.00	35	15.00	14.52	5078	37	a	5225	9.78
504-087	1932	I 227	022508.6	+275704	0	2.00 x 1.80		15.50	14.90	10495	82	a	10640	10.23
504-088			022510.8	+320813	1	0.70 x 0.25	73	15.10	14.47	5231	69	a	5383	9.82
523-048			022556.0	+375231	2	0.60 x 0.20	75	15.50	14.66	11254	50	a	11422	10.40
523-049	1960		022606.2	+381013	5	1.10 x 0.50	65	15.50	14.85	5148	60	e	5316	9.66
504-095	1964	N 940	022629.3	+312506	1	1.70 x 1.20	46	13.40	12.77	5231	35	a	5380	10.50
504-104	1991	N 953	022813.1	+292201	0	1.50 x 1.50		14.50	13.97	4728	45	a	4873	9.93
505-003			022944.3	+275101	3	0.65 x 0.45	48	15.70	15.10	4615	55	a	4755	9.50
505-005	2022		023018.0	+323200	0	1.00 x 0.80		15.20	14.80	5229	176	e	5378	9.69
505-008			023036.0	+324800	1	0.60 x 0.40	49	15.20	14.60	9764	92	a	9914	10.30
523-061	2040	N 968	023104.3	+341539	0	3.60 x 1.80		13.80	13.39	3608	54	a	3762	9.94
523-070			023311.9	+354411	1	0.50 x 0.25	62	15.70	15.00	9232	38	a	9389	10.09
523-088			023817.9	+364502	1	1.40 x 0.70	62	15.40	14.66	9043	60	a	9199	10.21
523-089	2169		023829.8	+370048	1	1.50 x 1.10	44	15.50	15.11	9192	76	a	9349	10.04
505-044	2203	N1066	024048.0	+321500	0	1.70 x 1.60		14.90	14.33	4362	60	a	4503	9.72
524-006			024118.0	+371700	1	0.80 x 0.50	52	15.70	14.96	9605	50	a	9760	10.14
505-048	2218		024154.0	+323000	5	1.10 x 1.10	0	15.40	14.94	5220	58	a	5361	9.63
505-049	2222		024206.0	+324700	5	1.20 x 0.70	55	14.90	14.18	4913	53	a	5055	9.88
505-050			024212.0	+320430	2	0.90 x 0.20	88	15.50	14.79	4933	54	a	5072	9.64
524-018	2244		024348.0	+392500	5	1.00 x 0.90	27	15.40	14.98	9374	60	a	9534	10.11
524-021			024448.0	+372200	1	0.80 x 0.50	52	15.60	14.86	9044	31	a	9197	10.13
524-023			024600.0	+361500	1	0.70 x 0.30	67	15.40	14.69	5022	37	e	5171	9.70
524-024	2288		024606.0	+350800	2	1.30 x 0.70	59	15.50	14.92	12373	78	a	12519	10.37
554-008	2298	I 257	024624.4	+464613	0	2.20 x 1.60		14.50	13.29	9240	47	a	9417	10.78
539-112	2322	N1106	024726.9	+412758	1	1.70 x 1.70	0	13.70	13.17	4407	26	e	4570	10.20
524-027	2328		024754.0	+371500	0	1.70 x 1.40		13.80	13.30	5026	56	a	5177	10.25
539-114	2335	I 262	024824.0	+423800	1B	2.10 x 1.70	37	14.80	14.21	5392	38	a	5557	9.95
524-031	2363		025036.0	+392300	5	1.60 x 1.40	30	14.60	13.96	5658	53	a	5813	10.09
540-015	2408	N1138	025319.0	+425048	1B	1.40 x 1.40	0	14.10	13.29	2240	32	a	2403	9.59
524-044	2481	I 278	025818.0	+373500	0	2.30 x 2.30		14.80	14.25	4929	51	a	5074	9.86
524-047	2493		025854.0	+353500	5	1.40 x 0.70	62	15.50	14.49	13118	183	a	13256	10.60
506-005	2506		030030.0	+273000	1	1.30 x 1.10	33	15.00	14.50	10731	51	a	10840	10.42
540-038	2533	N1198	030256.0	+413928	0	2.50 x 1.30		14.00	13.22	1558	29	a	1711	9.33
524-050		I1874	030313.1	+354927	2B	0.90 x 0.60	49	14.80	14.02	4966	60	e	5102	9.96
524-057			030517.6	+341043	1	0.60 x 0.40	49	15.70	15.04	6401	42	a	6530	9.76
540-046	2559		030558.8	+424658	1	1.60 x 0.70	66	14.50	13.13	5572	28	a	5726	10.41
524-059			030722.6	+345339	1B	0.75 x 0.30	69	15.40	14.62	6561	60	e	6691	9.95
524-061	2575	N1226	030754.0	+351200	0	2.30 x 1.80		14.50	13.63	6125	54	a	6255	10.29
524-064	2579		030818.0	+351700	0	1.20 x 0.80		15.70	14.83	5931	53	a	6061	9.78
525-012		I 305	031154.0	+374100	0	0.60 x 0.50		15.70	14.97	5066	41	a	5201	9.59
525-013		I1900	031248.0	+365900	1	0.80 x 0.55	48	15.00	14.17	5595	89	a	5728	9.99
525-015		I1902	0313 0.0	+370000	2	0.70 x 0.70	0	15.70	14.96	7055	60	e	7188	9.88
525-022			031741.2	+374133	7	0.80 x 0.65	37	15.40	14.59	5104	60	e	5235	9.75
525-032			0323 0.8	+375327	7	0.70 x 0.60	32	15.50	14.65	9084	60	e	9212	10.22
525-034	2745		032439.2	+361307	5	1.20 x 0.80	49	15.50	14.49	4325	62	a	4447	9.65
525-037	2761		032655.1	+381700	2	1.40 x 0.20	90	15.40	14.36	6131	27	a	6258	10.00
525-043			0331 0.0	+392600	5	0.60 x 0.30	62	15.00	13.68	5502	60	e	5630	10.18
525-042	2784		0331 2.2	+392246	1	1.60 x 1.20	43	14.30	13.26	6104	67	a	6232	10.43
525-044	2788		033136.0	+360300	0	1.40 x 0.80		15.70	14.78	4574	102	a	4690	9.58
526-005	2828		0339 6.0	+390500	5B	1.50 x 1.40	22	15.30	14.16	12296	70	a	12417	10.67
526-010			034818.0	+365600	1	0.60 x 0.40	49	15.70	14.67	5199	41	a	5307	9.73
526-011	2881		0349 0.0	+360500	1	1.50 x 1.00	49	15.00	13.73	5604	59	a	5708	10.17
487-001			0352 6.0	+272720	5	0.30 x 0.30	0	15.40	14.84	5590	64	a	5661	9.72
508-006			040048.0	+304200	0	0.60 x 0.60		15.10	14.30	5402	73	a	5478	9.91
526-017	2945		040124.0	+334000	2	1.50 x 1.10	44	15.20	14.00	5228	60	e	5315	10.00
	2957	I2027	040324.0	+365900	0	1.00 x 1.00		16.00	14.38	6246	59	a	6344	10.00
506-008	2980	I 359	040924.0	+273500	0	1.30 x 1.30		15.40	14.85	3814	63	a	3872	9.39
203-003	3407		060530.0	+420500	3	1.30 x 0.90	47	14.60	12.88	3610	36	e	3657	10.12
207-014	4150	N2493	0757 1.5	+395805	1B	2.20 x 2.20	0	13.10	12.72	3879	49	a	3877	10.24

© American Astronomical Society • Provided by the NASA Astrophysics Data System

1993AJ....105.1251W

TABLE 1. (continued)

CGCG	UGC	NGC/IC	RA	Dec	T	a x b	i	m_z	m_c	V_{sun}	σ	e/a	V_o	log L
493-015			215454.0	+303000	0	0.80 x 0.65		15.00	14.28	6758	80	a	7041	10.13
428-025	11889	I1427	220110.6	+145153	0	1.20 x 0.90		15.20	14.88	7725	56	a	7971	10.00
513-003	11892		220142.0	+354500	0	1.10 x 0.80		15.10	14.20	5638	29	a	5927	10.01
428-028			220336.4	+140324	1	0.65 x 0.45	47	15.50	14.90	18179	49	a	18422	10.72
513-007	11929		220729.1	+390215	1	1.00 x 0.70	47	14.40	13.40	4612	71	a	4903	10.17
513-008			220742.0	+375700	7	0.90 x 0.70	40	14.90	13.88	7092	203	a	7382	10.33
513-010			2208 4.0	+362430	7	0.90 x 0.50	58	15.50	14.48	6155	60	e	6444	9.97
513-011	11938	I5180	2209 0.0	+384000	0	1.00 x 0.80		14.80	13.94	5978	56	a	6269	10.17
513-012	11942	N7227	220918.0	+382800	1	1.30 x 0.60	65	15.00	14.12	6485	48	x	6774	10.16
513-013	11945	N7228	220939.1	+382700	3B	1.60 x 1.20	43	15.00	14.13	6486	48	a	6777	10.16
514-021	12013		222048.0	+354800	12	1.10 x 0.20	90	15.30	13.86	5354	77	a	5644	10.08
513-015	11950		221021.7	+382603	0	1.30 x 0.90		14.30	13.38	6102	55	a	6392	10.41
513-016			2211 6.0	+383500	6	0.85 x 0.25	78	15.40	13.99	6366	60	e	6656	10.20
513-017			221136.0	+364700	1	0.55 x 0.45	36	15.00	14.12	6350	71	y	6709	10.16
513-020	11963		221248.0	+370300	2	1.00 x 0.20	90	15.00	13.93	6557	61	a	6846	10.25
513-021		I1441	2213 6.0	+370300	5	0.90 x 0.30	75	15.30	14.00	5441	114	e	5729	10.06
530-019	11972	N7248	221443.7	+401520	1	1.80 x 0.90	62	13.60	12.64	4337	50	a	4628	10.42
514-013			221948.5	+352433	2	1.00 x 0.15	90	15.50	14.51	4951	69	a	5236	9.78
514-016	12006		222017.0	+365115	2B	1.50 x 0.80	59	14.50	13.55	6143	55	a	6430	10.35
514-017	12007		222030.0	+355700	5	1.40 x 1.10	39	15.30	14.62	4620	50	a	4906	9.68
514-021	12013		222049.0	+354817	5	1.10 x 0.20	90	15.30	13.86	5354	77	a	5639	10.11
514-024		N7273	222154.0	+355700	1	0.80 x 0.50	52	14.80	13.95	4923	66	a	5208	10.00
514-025		N7276	222200.0	+355000	0	0.45 x 0.45		15.00	14.27	5971	47	a	6256	9.92
514-033	12040		222448.0	+360600	1B	1.70 x 1.20	46	14.60	13.75	6302	60	y	6627	10.29
514-036			222612.0	+334500	0	0.60 x 0.60		14.90	14.22	6092	57	a	6374	10.07
514-037			222636.0	+385000	6	0.80 x 0.60	43	15.00	14.08	4631	60	e	4918	9.90
514-047			222824.0	+392200	1	0.65 x 0.20	77	15.30	14.31	5246	57	a	5534	9.91
514-048			222836.0	+361807	7	0.80 x 0.60	43	15.40	14.63	7916	60	e	8200	10.12
514-051			222917.8	+342720	3	1.35 x 0.55	69	15.40	14.58	6545	64	a	6827	9.98
514-054	12075		223036.0	+385800	7B	1.60 x 1.20	43	15.10	14.34	5481	60	e	5768	9.93
514-056			223054.0	+385400	2	0.70 x 0.70	0	15.50	14.75	4575	56	a	4862	9.62
514-067	12111	N7330	223441.7	+381716	0	1.80 x 1.70		13.60	12.89	5314	38	a	5599	10.49
514-073			223512.0	+351700	1	0.55 x 0.25	65	15.30	14.51	8633	29	y	8885	10.24
514-087			223642.0	+351100	1	0.60 x 0.40	49	15.40	14.68	9003	52	a	9284	10.21
495-013			223857.3	+332140	1	0.60 x 0.30	62	15.30	14.63	6494	46	a	6772	9.96
514-094			2239 0.0	+342200	1	0.70 x 0.50	45	14.80	14.06	6799	52	a	7078	10.22
514-100			223954.0	+354000	1	0.50 x 0.35	47	15.50	14.81	7164	52	a	7445	9.97
515-003	12179		224245.0	+334403	1	1.30 x 1.30	0	14.50	13.83	6947	34	a	7224	10.33
495-031			224638.0	+311937	1	0.40 x 0.30	43	15.50	14.92	9339	60	e	9611	10.15
495-033			224712.5	+320607	1	0.50 x 0.45	27	15.50	14.98	6193	56	a	6466	9.78
515-007	12215		224836.0	+343500	5	1.50 x 1.00	49	15.50	14.74	5957	53	a	6234	9.84
515-008	12216	N7395	224848.0	+364900	1	1.20 x 1.10	24	15.30	14.68	5567	56	a	5845	9.76
495-036	12214		224839.3	+310640	5	1.40 x 0.90	51	14.10	13.37	6575	33	a	6846	10.47
515-010			2251 6.0	+365400	1	1.00 x 0.60	54	15.00	14.26	5576	49	a	5855	9.98
496-012	12235		225142.0	+320600	1	1.10 x 0.70	51	15.10	14.54	6656	40	a	6928	10.01
496-014	12242		2252 3.9	+321110	0	1.30 x 1.30		14.50	13.88	6756	39	a	7028	10.29
496-020			225245.0	+315500	0	0.60 x 0.60		15.30	14.81	6558	46	a	6829	9.89
515-018	12292	N7449	225718.0	+385200	0	1.00 x 0.80		15.40	14.61	5189	113	a	5468	9.78
496-030	12297		225748.0	+310800	1	1.30 x 0.60	65	15.00	14.38	6377	39	a	6645	10.04
496-031			225815.5	+302817	2	0.80 x 0.30	71	15.10	14.46	6391	50	a	6658	10.01
496-040	12356		230324.0	+305000	5	1.00 x 1.00	0	14.60	14.16	6974	36	a	7240	10.20
515-024	12360	N7485	230341.8	+335020	1	1.20 x 0.60	62	14.20	13.39	5706	57	a	5977	10.35
515-026			2305 0.0	+360500	1	0.75 x 0.25	75	14.80	13.99	5064	47	a	5338	10.01
496-054	12414	N7512	230954.0	+305100	0	1.80 x 1.50		14.10	13.55	7064	32	a	7339	10.21
496-062			231157.0	+281023	1	0.50 x 0.50	0	15.40	15.00	6872	37	a	7130	9.85
496-063	12444		2312 3.5	+311638	5	1.00 x 0.90	27	14.50	13.86	6251	46	a	6515	10.23
496-068			231226.5	+324500	1	0.70 x 0.20	79	15.50	14.85	5089	20	e	5355	9.67
496-078			231548.0	+285733	0	0.90 x 0.75		15.30	14.90	6552	42	a	6810	9.85
497-012			2321 6.7	+285440	1	0.80 x 0.50	52	14.80	14.24	6195	36	y	6487	10.07
497-024			232542.5	+321207	1	1.00 x 0.80	38	15.50	15.06	4455	55	a	4715	9.47
497-046			233637.7	+314827	2	1.00 x 0.90	27	14.80	14.30	5074	50	a	5328	9.88
476-120			234025.2	+271140	2	0.70 x 0.60	32	15.00	14.56	7566	49	a	7809	10.11
476-123			2341 0.0	+270200	1	0.90 x 0.50	58	14.90	14.35	9031	64	a	9274	10.34
517-003			234736.0	+363500	1	0.55 x 0.20	72	15.50	14.77	11123	52	a	11381	10.35
498-027			2351 5.5	+285900	5	0.40 x 0.40	0	15.30	15.00	6928	50	a	7170	9.86
499-021	12867		235543.5	+290447	2	1.00 x 0.40	69	15.40	14.93	7019	59	a	7259	9.90
499-023			235554.0	+274500	1	0.90 x 0.65	45	15.50	15.07	9012	89	a	9249	10.05
499-028		I5370	235736.0	+322743	2	0.70 x 0.50	45	14.90	14.31	10357	25	a	10603	10.48
499-031		I5373	235754.7	+323017	5	0.50 x 0.30	54	15.10	14.44	9558	46	a	9804	10.35

Column(11)—Heliocentric velocity $V_{\rm Sun}$ in km s^{-1}. For emission line–derived redshifts, σ is the standard deviation of the mean for all the lines measured, or ± 60 km s^{-1}, which is the estimated error for a single line in this sample. For absorption line–derived redshifts, errors are estimated from the JKFOUR program, to a minimum acceptable value of ± 25 km s^{-1}.

Column (13)—A simple indicator of whether the spectral features used to derive the redshift were seen in emission (e) or absorption (a). For a handful of galaxies, velocities were derived from two absorption line spectra (x) and combining both absorption and emission lines (y).

Column (14)—Local Group velocity V_0 in km s^{-1} assuming a correction for the Sun's motion of 300 sin l cos b, where l and b are the galactic longitude and latitude.

Column (15)—Luminosity h^2L, in logarithmic solar units, derived from m_c and V_0.

2.2 H I Data

As part of the continuing H I line survey of spiral galaxies in the Pisces–Perseus supercluster, we have obtained 21 cm line spectra with two telescopes: the 305 m Arecibo telescope of the National Astronomy and Ionosphere Center and the (late) 91 m telescope of the National Radio Astronomy Observatory.[2] In this section, we present the results of observations of the 315 galaxies in this declination strip made by us during the course of this survey or other projects. The H I properties for some of the objects observed for other purposes have been previously published but are included here again for convenience. The objects and their properties are presented in Table 2.

The observations have been conducted in the standard observing modes appropriate for the individual telescopes. Survey observations with the Arecibo dual circular feed system are described in Giovanelli & Haynes (1985). Since the initial observations, improvements in receiver sensitivity, spectrometer capability, and feed tuning efficiency have substantially increased the speed in which the observations can be conducted. Spectra are the accumulated average of individually weighted total power ON–OFF pairs. Similarly, observations with the 91 m Green Bank telescope were also conducted in a total power mode and follow the general observing strategy outlined in Haynes *et al.* (1988).

Columns (1) to (10) of Table 2 are identical to the entries found in Table 1. Additional entries include:

Column (11)—21 cm line heliocentric velocity $V_{\rm Sun}$ in km s^{-1} measured as the midpoint of the emission profile at a level of 50% of the mean signal intensity.

Column (12)—Adopted Local Group velocity V_0 in km s^{-1} assuming a correction for the Sun's motion of 300 sin l cos b, where l and b are the galactic longitude and latitude. The adopted heliocentric velocity is the 21 cm velocity if the object is a high quality detection; if not, the optical velocity is adopted, when available.

Column (13)—Observed 21 cm profile width W_1 in km s^{-1}, measured at a level of 50% of the mean signal intensity.

Column (14)—Observed 21 cm profile width W_2 in km s^{-1}, measured at a level of 20% of the peak signal intensity.

Column (15)—21 cm profile width corrected for viewing inclination and to the rest frame of the observer, W_c, in km s^{-1}.

Column (16)—Observed 21 cm line flux $F_{\rm obs}$ in Jy km s^{-1}.

[2]The National Radio Astronomy Observatory is operated by Associated Universities Inc. under a management agreement with the National Science Foundation.

© American Astronomical Society • Provided by the NASA Astrophysics Data System

Column (17)—21 cm line flux F_c in Jy km s^{-1} after correction for pointing, beam dilution, and internal absorption following HG84.

Column (18)—rms noise in baseline 21 cm line profile σ in mJy, where available.

Column (19)—Signal-to-noise ratio of H I emission spectrum, measured as the ratio of peak signal flux to σ, where available.

Column (20)—Logarithm of optical luminosity in solar units, $\log_{10}(h^2 L)$, with $h = H_0/100$ km s^{-1}-Mpc^{-1}.

Column (21)—Logarithm of H I mass in solar units, $\log_{10}(h^2 \mathcal{M}_H)$.

Column (22)—Telescode identification code for H I observations: 0—Arecibo 305 m with dual circular feed, 1—Green Bank 91 m, 2—Effelsberg 100 m, and *B*—Arecibo 305 m with linear feed major axis mapping.

TABLE 2. Parameters of objects observed at 21 cm.

CGCG	UGC	NGC/IC	RA	Dec	T	a x b	i	m_z	m_c	V_{sun}	V_o	W_1	W_2	W_c	F_{obs}	F_c	rms	snr	log L	log M_H	I	Q	Ref
	11837		215006.0	+355153	7	1.40 x 0.90	51	16.0	14.72	5337	5627	345	320	446	3.42	3.98	1.78	7.9	9.76	9.47	0	3	1
	11841		215042.3	+384207	12	3.00 x 0.20	90	16.5	13.46	5989	6282	535		524	12.91	13.40	3.06	14.1	10.36	10.10	1	1	2
	11862		215538.6	+384130	8	1.80 x 0.20	90	16.5	14.47	5847	6139	383		376	5.67	5.75	2.19	10.4	9.94	9.71	1	3	2
	11893		220157.2	+354147	7	2.30 x 0.30	90	16.0	14.21	5564	5852	619	607	610	7.28	9.11	1.93	8.4	10.00	9.87	0	1	1
	11903		220307.4	+344447	5B	1.00 x 1.00	0	16.0	15.23	4784	5071	109	94		1.20	1.36	1.81	8.9	9.47	8.92	0	1	1
	11945	N7228	220939.1	+382700	3B	1.60 x 1.20	43	15.0	14.13	6553	6843	432		625	4.00	4.07	2.28	7.4	10.17	9.65	1	1	2
513-018	11955		221136.0	+385900	7	1.20 x 0.60	62	14.7	13.48	5360	5650	134		153	7.00	7.05	3.90		10.26	9.73	1	1	4
514-005			221418.0	+361243	12	0.55 x 0.50	25	15.6	14.87	5895	6182	378	294		1.89	2.03	2.22	4.5	9.78	9.26	0	3	1
514-006	11975		221507.4	+351910	2	1.60 x 1.20	43	15.2	14.49	6305	6591	319	267	462	5.19	6.29	1.54	16.2	9.99	9.81	0	3	1
514-008			221725.0	+351610	3B	0.70 x 0.50	45	15.6	14.86	5744	6029	383	295	527	1.55	1.67	1.21	5.5	9.76	9.16	0	2	1
514-011			221903.4	+341953	12	0.60 x 0.45	43	15.5	14.79	6413	6697	274	252	401	1.88	2.02	1.30	6.6	9.88	9.33	0	1	1
514-012		N7263	221936.0	+360600	2	0.80 x 0.60	43	15.7	14.93	6205	6491	322	269	466	0.54	0.59	1.62	3.5	9.80	8.77	0	2	1*
514-014	12001	N7264	222000.5	+360807	5	2.20 x 0.30	90	14.7	12.90	4269	4555	534	504	526	1.97	2.43	1.10	6.7	10.30	9.08	0	3	1
	12008		222026.1	+372512	7	1.00 x 0.90	27	16.0	15.41	7472	7759	259	245		3.38	3.80	2.27	8.3	9.76	9.73	0	1	1*
514-018	12009		222028.0	+374329	12	1.50 x 0.80	59	13.8	12.85	1238	1525	202	189	236	7.53	8.78	3.53	12.4	9.37	8.68	0	1	1
514-020	12012		222048.8	+353353	5	1.00 x 0.60	54	15.3	14.48	4776	5060	358	322	439	1.13	1.25	0.75	5.7	9.76	8.88	0	1	1*
514-023	12020		222133.2	+350810	3B	1.30 x 1.10	33	15.6	14.94	6025	6309	363	335	649	2.41	2.81	1.51	8.6	9.77	9.42	0	1	1
514-030	12037		222422.4	+362927	5B	1.50 x 1.30	31	15.5	14.84	6042	6327	144	129	278	2.28	2.76	2.18	8.8	9.82	9.42	0	1	1
514-032	12039		222433.8	+351553	5B	1.70 x 1.20	46	14.1	13.22	6013	6297	530	457	729	6.52	8.00	1.62	11.6	10.46	9.87	0	1	1
514-034	12044		222535.4	+382000	4	1.80 x 0.70	70	15.5	14.51	5442	5729	464	446	487	6.84	8.17	3.56	7.3	9.86	9.80	0	1	1
514-039	12051		222703.9	+372947	6B	1.00 x 0.90	27	15.1	14.49	8785	9070	251	140		1.43	1.61	1.91	5.5	10.27	9.49	0	3	1*
514-042	12056		222737.8	+362750	3	1.60 x 1.00	52	15.5	14.74	7485	7769	376	359	464	4.11	4.90	1.56	9.5	10.03	9.84	0	1	1
514-049	12063		222855.6	+350703	4	1.50 x 0.50	75	15.6	14.51	6690	6973	444	407	453	3.44	3.95	1.74	9.7	10.03	9.66	0	1	1
514-053	12073		223018.0	+385800	5B	2.20 x 0.80	72	14.8	13.60	4676	4962	435		455	12.58	12.87	6.51		10.10	9.87	1	1	2
514-054	12075		223036.0	+385800	7B	1.60 x 1.20	43	15.1	14.34	5341	5627	223		331	11.18	11.37	3.16		9.91	9.93	1	1	2
514-058			223250.7	+365627	7	0.65 x 0.55	33	15.3	14.68	4856	5139	234	175	429	1.61	1.74	1.94	6.0	9.70	9.03	0	3	1
514-068	12113	N7331	223447.7	+340935	5	11.40 x 4.00	73	10.4	9.50	819	1099	527		555		187.80			10.43	9.73	B	1	4
514-069	12116	N7335	223502.8	+341123	2	1.40 x 0.60	67	14.7	13.98	6298	6578						1.05		10.19		0	0	1
514-071	12120	N7337	223509.8	+340700	3B	1.20 x 1.00	35	15.7	15.22	6617	6897	274	244	472	0.60	0.69	1.03	4.9	9.74	8.89	0	3	1*
514-076	12126	N7342	223556.8	+351427	3B	1.50 x 1.40	22	15.3	14.83	8075	8356	358	335		1.33	1.63	1.50	5.0	10.06	9.43	0	3	1
514-077			223604.6	+354200	3	0.70 x 0.60	32	15.7	15.06	8680	8961	365	302	670	3.94	4.27	3.37	4.9	10.03	9.91	0	3	1
514-082	12129	N7343	223619.6	+334845	5B	1.00 x 0.80	38	14.3	13.67	7469	7747	365	338	584	5.26	5.87	2.19	8.8	10.46	9.92	0	1	1*
514-086	12132		223633.3	+340240	5B	1.00 x 0.50	62	15.4	14.63	6127	6406	342	321	384	1.04	1.14	1.04	5.3	9.91	9.04	0	3	1
514-089			223727.2	+340713	7	0.90 x 0.60	49	15.2	14.63	7439	7718	96	61	127	3.52	3.87	2.16	24.5	10.07	9.74	0	3	1
514-090	12137		223734.2	+375718	6B	1.90 x 1.60	34	14.0	13.26	4685	4968	176	147	318	5.25	6.84	3.77	12.2	10.24	9.60	0	1	1*
514-095	12155		223912.0	+350020	5B	1.10 x 0.40	72	15.4	14.48	8707	8987	442	413	456	1.16	1.28	0.86	6.4	10.26	9.39	0	3	1
	12156		223912.0	+390200	7B	1.10 x 1.10	0	14.8	14.13	5182	5467	166			3.74	3.78	3.10		9.97	9.43	1	3	2
514-102		N7363	224059.5	+334407	7	0.90 x 0.90	0	14.6	14.06	6722	6999	276	258		1.57	1.75	1.23	6.8	10.21	9.31	0	1	1
514-103	12173		224135.8	+380643	7	2.10 x 1.30	53	13.7	12.79	4777	5060	382		483	5.45	7.08	2.11		10.44	9.63	0	1	5
514-104		N7369	224154.0	+340510	7	1.00 x 0.90	27	14.8	14.16	6578	6856	454	442		4.37	4.91	2.33	6.1	10.16	9.74	0	3	1
515-005	12181		224352.5	+374719	7	1.10 x 0.90	36	14.5	13.66	4758	5039	156	139	265	3.55	4.02	3.23	9.2	10.09	9.38	0	1	1
	12192		224618.3	+365610	12	1.00 x 0.90	27	17.0	16.38	6487	6766	95	79		2.18	2.45	4.48	6.7	9.26	9.42	0	1	1
515-006	12201		224650.7	+344340	4	1.60 x 0.30	90	15.0	13.76	5055	5331	408	393	401	2.01	2.31	0.75	11.0	10.10	9.19	0	1	1
	12227		225031.6	+341220	7	1.10 x 0.90	36	16.5	15.89	6438	6713	113	102	191	3.58	4.06	2.98	13.4	9.45	9.63	0	1	1
	12236		225138.1	+355833	12	1.60 x 1.60	0	16.5	16.03	5588	5864	105	86		2.47	3.11	2.92	11.3	9.27	9.40	0	1	1
	12248		225230.0	+361620	10	1.00 x 0.90	27	16.5	16.04	4880	5157	129	88		2.06	2.32	1.32	16.5	9.16	9.16	0	1	1
515-011			225255.0	+362407	7	0.70 x 0.50	45	14.8	14.03	5660	5937	440	383	619	2.24	2.42	1.12	8.0	10.08	9.30	0	3	1
515-013			225404.9	+355820	5	0.75 x 0.20	81	15.6	14.43	5082	5358	330	227	332	1.48	1.59	1.41	6.3	9.83	9.03	0	3	1
515-014	12260		225412.4	+372753	7	1.70 x 0.30	90	15.7	14.19	5540	5818	304		302	4.02	4.69	3.00	7.5	10.00	9.57	0	3	3
515-015	12276	N7440	225612.0	+353207	3B	1.70 x 1.70	0	14.6	13.94	5659	5934	145	119		3.20	4.12	2.03	14.1	10.12	9.53	0	1	1
515-021	12331		230038.0	+342737	7	1.00 x 0.60	54	15.5	14.87	5794	6066	272	259	336	2.30	2.54	1.39	9.8	9.77	9.34	0	1	1
515-022			230126.1	+344300	7	1.00 x 0.60	54	15.1	14.34	5761	6033	153	120	189	1.83	2.02	1.44	10.5	9.97	9.24	0	1	1
515-023			230234.7	+354500	7	0.75 x 0.50	49	15.0	14.29	5822	6095	308	242	408	2.40	2.60	1.55	8.6	10.00	9.36	0	1	1
	12358		230324.1	+335300	6	1.00 x 0.20	90	16.0	14.77	5338	5608	339	227	337	0.75	0.82	0.90	4.8	9.74	8.78	0	3	1
515-025	12372		230438.1	+353025	12	0.80 x 0.70	30	14.5	13.86	5480	5752	274			3.96	4.34	2.80	7.5	10.12	9.53	0	3	3
	12375		230449.6	+345913	12	1.20 x 0.50	68	16.0	15.23	5526	5797	288	269	308	3.06	3.42	2.69	5.6	9.58	9.43	0	3	1
	12401		230803.6	+340740	9	1.00 x 0.80	38	17.0	16.66	5502	5771	116	90	189	1.76	1.97	2.30	7.9	9.01	9.19	0	1	1
	12415	N7514	231001.6	+343655	2	1.60 x 1.00	52	13.5	12.87	4843	5112	323		402	2.19	2.61	1.90	6.5	10.42	9.21	0	3	3
516-001			231051.8	+361127	6	0.65 x 0.25	71	15.5	14.58	5287	5558	338	222	358	1.35	1.44	1.45	5.5	9.81	9.02	0	3	1
516-002	12474		231418.1	+334325	3	1.20 x 0.40	75	14.1	13.33	5117	5383	368	324	375	1.15	1.28	1.47	3.2	10.28	8.94	0	2	1*

© American Astronomical Society • Provided by the NASA Astrophysics Data System

1993AJ....105.1251W

1993AJ....105.1251W

TABLE 2. (continued)

CGCG	UGC	NGC/IC	RA	Dec	T	a x b	i	m_z	m_c	V_{sun}	V_o	W_1	W_2	W_c	F_{obs}	F_c	rms	snr	log L	log M_H	I	Q	Ref
516-003	12528		231754.5	+351300	6	1.20 x 0.40	75	15.3	14.42	8034	8301	415	363	426	3.55	3.95	1.91	9.1	10.22	9.81	0	1	1
516-004			232452.3	+365647	6	0.65 x 0.60	23	14.8	14.19	5094	5360	272	249		2.01	2.17	1.70	5.5	9.93	9.17	0	2	1
	12612		232552.9	+350143	7	1.00 x 0.10	90	17.0	15.46	10030	10294	422	340	408	2.33	2.54	1.45	6.2	9.99	9.80	0	3	1
	12617		232611.5	+350900	12	1.00 x 0.30	78	16.5	15.44	9994	10258	441	413	442	2.07	2.26	1.48	6.2	9.99	9.75	0	3	1
	12627		232643.0	+344612	2	1.00 x 0.35	73	16.0	15.31	9934	10196	521	493	526	1.14	1.25	0.78	6.4	10.04	9.49	0	3	1
	12651		232941.2	+350636	12	1.00 x 0.80	38	16.5	15.92	6488	6751	296	281	475	4.61	5.15	1.83	12.5	9.44	9.74	0	1	1
516-006	12672		233154.8	+342053	7	1.10 x 0.80	44	14.6	13.90	6516	6776	181	160	259	2.08	2.34	1.72	9.1	10.25	9.40	0	1	1
	12697		233333.3	+353920	9	1.00 x 0.60	54	17.0	16.50	5207	5468	215	204	266	3.51	3.88	1.75	11.1	9.02	9.44	0	1	1
	12743		233934.9	+355026	12B	1.00 x 0.40	69	16.5	15.48	10531	10790	335	247	350	2.64	2.89	2.11	5.6	10.02	9.90	0	1	1
517-004			234745.7	+362343	5	0.75 x 0.20	81	15.4	14.27	11186	11443	465	406	459	2.26	2.43	1.90	5.4	10.56	9.88	0	1	1
	12807		234827.3	+353010	12	1.00 x 0.10	90	17.0	15.41	12340	12595	414	389	397	2.85	3.11	1.67	7.8	10.18	10.07	0	1	1
517-005			234928.0	+333210	12	0.40 x 0.35	30	15.6	15.13	12610	12861	161	161		0.71	0.75	1.15	5.2	10.32	9.47	0	2	1
517-010			235748.5	+342017	7	0.60 x 0.50	35	15.5	15.02	12702	12951	173	148	298	0.75	0.81	1.13	5.7	10.37	9.50	0	1	1
517-013	12909	I5376	235847.2	+341447	4	2.10 x 0.40	90	14.7	13.58	5029	5277	446	431	438	5.55	6.76	2.79	7.7	10.16	9.65	0	1	1
517-014			235924.7	+362210	2	0.60 x 0.30	62	15.4	14.77	9714	9965	107	107		-0.77		0.96		10.24		0	4	1*
518-013	63		000516.1	+354124	9	1.00 x 0.70	47	15.6	15.37	439	686	71	44	100	1.96	2.18	2.48	16.1	7.67	7.38	0	1	1
518-015	73	N 11	000606.9	+371021	3	1.60 x 0.22	90	14.5	13.46	4389	4639	454	381	447	2.12	2.44	3.21	3.9	10.10	9.09	0	1	1
518-017			000807.1	+353406	5	0.75 x 0.40	59	15.5	14.80	6159	6404	166	115	191	2.17	2.34	2.38	8.3	9.84	9.36	0	1	1
	128		001114.8	+354300	8	2.30 x 2.00	30	16.5	16.23	4537	4781	233	223		8.27	11.85	3.40	13.7	9.02	9.81	0	1	1
	160		001426.7	+341320	8	1.60 x 1.50	21	16.5	16.31	4671	4911	147	128		3.73	4.66	2.60	12.2	9.00	9.42	0	1	1
518-022			001436.0	+353630	7	0.85 x 0.50	55	15.7	15.05	11814	12056	223	223	267	0.87	0.95	1.13	5.1	10.29	9.51	0	1	1
	222		002028.9	+345213	12	1.20 x 0.10	90	18.0	16.46	6110	6347	212	197	208	0.94	1.04	1.41	4.9	9.17	9.00	0	1	1
519-007			002136.6	+361834	10	0.70 x 0.40	56	15.7	15.17	15677	15917	263	248	303	1.16	1.25	2.33	3.4	10.48	9.87	0	2	1*
	344		003209.4	+391611	7	1.20 x 0.70	55	15.4	14.92	5780	6020	243		295	5.73	5.78	2.33		9.74	9.69	1	1	2
519-014			003430.8	+353740	5	0.60 x 0.20	75	15.5	14.58	4423	4654	151	94	156	1.57	1.67	1.89	8.5	9.65	8.93	0	1	1
519-015			003648.6	+360410	2	0.80 x 0.30	71	14.9	14.25	4391	4623	122	95	127	1.30	1.40	1.61	8.3	9.78	8.85	0	1	1
519-017	440	N 218	003902.7	+360507	12	1.30 x 1.20	23	15.5	15.23	4894	5125	97	62		4.69	5.53	3.42	20.2	9.48	9.53	0	1	1
519-018			003911.2	+364937	7	0.65 x 0.65	0	15.7	15.30	10889	11120	241	211		2.35	2.55	1.35	10.0	10.12	9.87	0	1	1
519-019	444		003922.1	+363149	12	1.20 x 0.80	49	14.0	13.43	4397	4627	528	484	696	4.40	4.99	1.81	6.6	10.11	9.40	0	1	1
519-021	480		004348.3	+360315	12	1.60 x 1.10	48	13.6	13.01	11220	11448	521	30	689	3.93	4.73	1.10	9.5	11.06	10.17	0	1	1*
520-002	549		005156.2	+363017	7	1.10 x 0.10	90	15.7	14.26	6035	6258	283		277	1.79	1.97	1.10	8.0	10.04	9.26	0	3	3
520-003	564		005229.5	+350950	12	1.00 x 0.70	47	15.7	15.27	11042	11263	391	360	525	3.40	3.78	1.97	7.2	10.14	10.05	0	3	1
520-004	602		005537.7	+362740	7B	1.70 x 1.60	20	14.5	14.10	6145	6366	279			5.13	6.54	1.20	24.0	10.12	9.80	0	1	3
520-006	614		005650.4	+351729	7B	1.60 x 1.00	52	14.0	13.43	2341	2559	228	198	292	4.21	5.04	3.25	7.3	9.59	8.89	0	1	1
520-008			005945.3	+340024	5	0.60 x 0.20	75	14.9	13.88	11322	11536	323	303	326	2.95	3.14	1.49	8.0	10.72	9.99	0	1	1
520-010			010300.0	+344306	6	0.55 x 0.25	65	15.4	14.64	12052	12264	426	405	459	2.09	2.23	1.28	7.0	10.47	9.90	0	3	1
520-011			010333.9	+333010	5	0.55 x 0.40	44	15.1	14.58	4561	4771	161	107	229	1.58	1.69	1.59	8.6	9.67	8.96	0	3	1
520-014	690		010443.6	+390756	7	2.50 x 1.90	42	13.8	13.26	5849	6071	367		553	8.00	8.34	3.40		10.41	9.86	1	1	4
520-015			010449.8	+334553	2	0.70 x 0.40	56	15.6	15.14	4530	4739	198	184	234	2.11	2.27	1.25	13.0	9.44	9.08	0	1	1
	713		010615.7	+373520	12	1.10 x 1.00	25	16.5	16.14	8341	8558	190	125		2.66	3.03	2.87	7.4	9.56	9.72	0	3	1
520-021	738		010818.0	+333420	8	1.30 x 1.00	41	15.5	15.16	4545	4752	171	152	263	1.12	1.30	1.65	5.8	9.44	8.84	0	1	1
	745		010841.4	+362443	7	1.00 x 0.40	69	16.5	15.81	9629	9842	243	228	257	1.15	1.26	1.68	5.0	9.81	9.46	0	1	1
520-022	748		010855.8	+350034	12	2.00 x 0.70	73	15.3	14.53	4857	5068	327	310	340	9.39	11.49	4.01	9.3	9.75	9.84	0	1	1
520-023	755		010949.4	+381420	7	1.50 x 1.50	0	14.6	14.16	6457	6674	227	211		5.98	7.39	7.82	4.6	10.13	9.89	0	3	1*
520-026	758	N 425	011012.5	+383013	12	1.00 x 0.90	27	13.5	13.00	6438	6654	291	260		2.87	2.89	2.47	6.9	10.59	9.48	1	3	1*
	764		011024.5	+344153	7	1.10 x 0.10	90	17.0	15.61	4736	4944	218	199	214	1.28	1.41	1.62	5.8	9.29	8.91	0	1	1
520-031			011134.5	+334750	7	0.80 x 0.60	43	15.7	15.24	4237	4442	114	64	170	0.90	0.98	1.62	9.0	9.35	8.66	0	3	1
520-032			011220.6	+333147	6	0.80 x 0.40	62	15.3	14.65	4440	4644	181	167	206	0.73	0.79	1.02	5.3	9.62	8.60	0	3	1
520-033	809		011300.0	+333300	7	1.40 x 0.20	90	14.8	13.55	4204	4408	325	307	322	4.89	5.52	1.38	14.4	10.02	9.40	0	1	1
520-036	831		011519.1	+381047	6	1.40 x 1.00	45	15.1	14.60	7286	7499	171	119	238	3.54	4.15	3.16	10.6	10.06	9.74	0	3	1*
521-003			011807.6	+344330	5	0.55 x 0.45	36	14.8	14.26	4590	4793	233	217	393	0.88	0.94	1.33	5.6	9.81	8.71	0	3	1
521-005	879	I1675	011810.8	+335921	12	0.80 x 0.25	76	14.3	13.31	5100	5301	426	339	436	0.89	0.96	1.25	4.2	10.27	8.80	0	2	1
521-006			011826.2	+362520	6	0.85 x 0.20	85	15.4	14.33	5029	5236	270	246	271	2.17	2.34	1.99	5.3	9.85	9.18	0	3	1
521-007	909		011910.1	+370826	7	1.70 x 1.10	51	14.4	13.72	5084	5293	279	255	363	6.59	8.03	2.23	14.2	10.11	9.72	0	1	1
521-008	913		011925.4	+342428	10	0.55 x 0.30	58	14.4	14.02	5124	5326	378	241	441	3.56	3.79	2.19	7.3	9.99	9.40	0	3	1
521-010	916	I1683	011949.2	+341035	12	1.70 x 0.70	68	14.2	13.38	4869	5071	416	371	445	1.02	1.21	0.91	4.9	10.20	8.86	0	3	1
521-013			012012.0	+335220	10	0.55 x 0.25	65	15.7	15.34	5125	5324	181	126	198	1.14	1.21	1.31	7.9	9.46	8.91	0	3	1
521-016	940		012048.0	+341833	7	1.10 x 0.80	44	14.9	14.45	6996	7197	310	288	443	3.29	3.70	1.86	7.2	10.08	9.66	0	1	1
521-018	944	N 512	012110.5	+333854	4	1.70 x 0.35	90	14.0	12.90	4857	5056	550	532	543	4.05	4.71	1.52	7.2	10.39	9.45	0	1	1*
521-017			012112.6	+333627	8	0.70 x 0.70	0	14.9	14.58	5145	5344	158	134		0.79	0.86	1.05	6.7	9.77	8.76	0	3	1*

© American Astronomical Society • Provided by the NASA Astrophysics Data System

1993AJ....105.1251W

TABLE 2. (continued)

CGCG	UGC	NGC/IC	RA	Dec	T	a x b	i	m_z	m_c	V_{sun}	V_o	W_1	W_2	W_c	F_{obs}	F_c	rms	snr	log L	log M_H	I	Q	Ref
521-020	953	N 513	012137.3	+333223	7	0.75 x 0.35	64	13.4	12.66	5859	6057	541	531	601	1.16	1.25	0.62	5.4	10.65	9.03	0	3	1
521-021	975		012224.9	+340555	12	1.20 x 0.80	49	15.0	14.49	4897	5097	269	258	354	2.14	2.43	2.05	5.5	9.77	9.17	0	1	1
521-022	979	N 523	012231.0	+334555	10	3.20 x 0.80	83	13.5	13.11	4761	4959	509	477	511	11.55	16.57	2.12	14.9	10.29	9.98	0	1	1
521-024	1012	N 531	012328.4	+342940	2B	1.90 x 0.50	81	14.9	14.34	4660	4860						1.50		9.78		0	0	1
521-025	1013	N 536	012331.4	+342635	5B	3.40 x 1.70	62	13.2	12.52	5189	5388	556	307	627	9.92	15.94	1.92	18.6	10.60	10.04	0	1	1
521-028			012411.0	+334136	5	0.70 x 0.30	67	15.6	14.84	4080	4277	347	328	376	1.47	1.58	1.44	5.7	9.47	8.83	0	3	1
521-030	1034	N 551	012448.5	+365526	6B	2.00 x 0.80	69	13.5	12.67	5189	5392	377	356	403	2.66	3.28	2.78	6.6	10.55	9.35	0	1	1
521-031	1046		012512.0	+375723	8	1.60 x 1.60	0	15.7	15.38	5224	5429	145	131		4.62	5.83	3.79	11.1	9.46	9.61	0	1	1
521-032	1048	N 561	012527.9	+340303	3B	1.70 x 1.50	29	14.1	13.65	4670	4868	244	221		2.64	3.33	1.52	9.2	10.06	9.27	0	1	1
	1054		012557.3	+340508	7	1.40 x 0.12	90	17.0	15.58	2663	2861	183	172	181	3.54	3.99	2.75	10.0	8.83	8.89	0	1	1
521-036	1059		012618.0	+391000	12B	1.60 x 1.00	52	14.7	14.02	8269	8478	180		224	5.27	5.35	3.80		10.40	9.96	1	1	2
521-038			012649.2	+333420	8	0.90 x 0.60	49	15.6	15.17	6575	6770	148	120	196	2.27	2.49	2.75	7.5	9.74	9.43	0	3	1
521-040	1086		012843.1	+343133	12	1.00 x 0.35	73	15.0	14.20	4163	4359	224	210	233	4.33	4.74	2.01	11.6	9.75	9.33	0	1	1
521-041	1088		012844.7	+363530	7	1.70 x 1.60	20	15.7	15.45	4894	5095	133	123		1.53	1.95	2.58	6.5	9.38	9.08	0	1	1
521-045	1100	N 587	012941.6	+350608	5	2.20 x 0.80	72	13.7	12.86	4530	4728	452	433	473	4.14	5.22	1.45	14.3	10.35	9.44	0	1	1
521-046	1111	N 591	013039.3	+352443	2B	1.40 x 1.10	39	14.5	14.07	4547	4744	201	188	311	2.66	3.13	1.81	8.7	9.87	9.22	0	1	1
521-047	1125		013157.6	+334650	10	0.65 x 0.55	33	14.3	13.93	4455	4647	263	188	478	2.61	2.82	1.30	10.9	9.91	9.16	0	3	1
521-051	1131		013224.0	+341300	8	1.40 x 1.20	32	15.4	15.17	5090	5284	120	107	228	1.75	2.08	2.76	8.7	9.53	9.14	0	3	1
521-057			013505.5	+343410	7B	0.80 x 0.55	48	15.5	15.39	4650	4842	214	186	292	1.61	1.75	2.37	5.6	9.36	8.99	0	3	1
521-060	1164	N 634	013525.0	+350641	3	2.20 x 0.70	76	14.0	13.15	4942	5136	520	492	527	6.79	8.47	2.43	9.8	10.31	9.72	0	1	1
521-061	1166		013542.0	+344421	2	1.50 x 0.45	78	14.0	13.21	4872	5064						2.50		10.27		0	0	1
521-062			013639.2	+333426	6	0.75 x 0.45	54	15.5	15.34	4838	5026	190	180	234	1.37	1.48	1.65	5.5	9.41	8.95	0	1	1
521-063			013639.3	+345416	6	1.00 x 0.20	90	15.4	14.64	5162	5353	166	147	165	1.39	1.52	1.25	8.4	9.75	9.01	0	1	1
521-064			013704.3	+340920	5	0.80 x 0.60	43	14.9	14.47	4257	4448	191	178	282	3.30	3.60	1.28	15.9	9.66	9.23	0	1	1
521-066	1178		013735.5	+342220	7	2.00 x 0.35	90	14.8	13.77	5500	5690	388	361	385	11.38	13.75	3.05	14.6	10.15	10.02	0	1	1
521-068			013822.4	+343327	5	1.00 x 0.70	47	14.7	14.11	5091	5281	123	109	169	3.32	3.69	2.14	15.7	9.95	9.39	0	1	1
521-072	1212		014114.7	+340813	5	1.70 x 1.40	36	14.5	14.01	10748	10936	346	330	579	4.21	5.25	1.47	12.9	10.62	10.17	0	1	1
521-073	1220	N 662	014139.4	+372643	4	0.80 x 0.45	57	13.6	12.63	5662	5857	291		342	2.78	3.01	1.90		10.63	9.39	0	1	3
521-074			014144.4	+342437	5	0.80 x 0.25	76	15.0	14.17	5677	5864	193	165	197	1.05	1.13	1.01	7.3	10.02	8.96	0	3	1
521-078	1234		014257.5	+345130	7	1.20 x 0.70	55	14.8	14.36	5652	5839	257	240	313	4.08	4.61	2.26	9.3	9.94	9.57	0	1	1
522-001	1238	N 668	014327.5	+361238	5	2.20 x 1.60	44	13.5	12.64	4496	4687	318	298	453	6.80	9.19	2.82	11.0	10.44	9.68	0	1	1
522-002			014333.8	+344043	5	0.80 x 0.50	52	14.7	14.22	5543	5729	256	122	321	3.00	3.26	1.48	13.6	9.98	9.40	0	3	1
522-003			014402.4	+343122	12	0.50 x 0.40	38	15.2	14.97	4209	4395	233	212	377	0.97	1.03	1.05	6.5	9.45	8.67	0	3	1
522-004	1248	N 669	014421.0	+351850	4	3.30 x 0.70	90	12.9	11.57	4656	4844	796	749	787	1.57	2.26	0.60	6.0	10.89	9.10	0	1	1
522-005	1251		014435.4	+354713	10	1.00 x 0.50	62	15.0	14.87	4845	5033	310	297	350	0.46	0.51	0.82	3.9	9.60	8.48	0	3	1
522-006			014449.9	+344627	7	0.90 x 0.90	0	15.0	14.91	5556	5741	116	95		4.38	4.89	2.30	23.7	9.70	9.58	0	1	1
522-007	1257		014511.2	+361213	4	1.10 x 0.55	62	15.0	14.59	4660	4850	352	339	396	1.78	1.98	1.39	6.7	9.68	9.04	0	1	1
522-013			014629.7	+344332	5	0.50 x 0.45	27	15.5	15.47	4025	4209	194	150		4.94	5.28	1.58	23.5	9.21	9.34	0	1	1
522-014	1277		014630.6	+351216	2	2.00 x 1.20	54	14.5	14.03	4143	4330	497	476	604	3.03	3.84	1.62	6.7	9.81	9.23	0	1	1
522-017	1298	N 687	014737.7	+360725	1	1.40 x 1.40	0	13.3	12.52	5147	5335						1.27		10.59		0	0	1
522-018	1299		014737.8	+350647	9	1.00 x 0.60	54	15.7	15.69	5496	5682	184	166	228	3.43	3.79	2.13	10.2	9.38	9.46	0	1	1
522-020	1302	N 688	014749.1	+350215	5B	2.60 x 1.70	50	13.3	12.43	4151	4337	360	337	468	9.26	13.34	2.68	15.5	10.45	9.77	0	1	1
522-021	1307		014751.8	+354107	12	1.70 x 0.50	78	15.1	14.41	4889	5075						0.90		9.79		0	0	1
	1316		014824.0	+343600	12	1.40 x 0.80	56	16.5	16.07	4690	4873	232	220	277	3.40	3.93	2.02	11.2	9.10	9.34	0	1	1*
522-024	1319		014833.1	+354906	12	0.90 x 0.60	49	14.5	13.83	5311	5496	278	258	365	1.42	1.56	1.37	5.7	10.10	9.05	0	1	1
522-025			014906.5	+355300	6	0.90 x 0.60	49	15.6	15.49	6050	6235	230	175	303	0.46	0.51	0.97	3.7	9.54	8.67	0	3	1
	1330		014911.4	+344730	12	1.30 x 1.30	0	16.0	15.86	4382	4564	114	96		2.33	2.77	1.96	12.8	9.12	9.13	0	1	1
522-031	1338		014925.7	+353300	5	1.00 x 0.80	38	15.2	15.08	4099	4284						0.87		9.38		0	0	1
522-035	1344		014938.1	+361522	3B	1.70 x 0.80	64	14.0	13.19	4398	4585						0.92		10.20		0	0	1
522-036	1345	N 705	014945.4	+355351	2	1.20 x 0.25	90	14.5	13.73	4526	4711						0.95		10.00		0	0	1
522-038	1347		014949.7	+362230	7	1.40 x 1.20	32	13.9	13.23	5542	5729	144	127	273	5.55	6.60	3.26	14.5	10.37	9.71	0	1	1
522-041	1349		014957.6	+354821	7	1.70 x 1.70	0	14.3	13.79	6107	6291	233	127		1.95	2.51	1.93	6.2	10.23	9.37	0	3	1
522-042	1350		015000.7	+361607	5B	2.10 x 1.50	45	14.5	13.86	5244	5431						1.00		10.07		0	0	1
522-047	1358	N 714	015032.9	+355833	2	1.60 x 0.35	90	13.9	12.96	4470	4654						1.10		10.30		0	0	1
522-049			015053.7	+361907	8	1.00 x 0.60	54	15.3	15.10	4670	4856	226	178	280	1.05	1.16	1.31	5.9	9.48	8.81	0	3	1
522-050	1361		015056.2	+362027	7	1.20 x 0.40	75	15.7	15.43	5746	5932	225	187	234	1.98	2.21	1.56		9.52	9.26	0	1	1
522-055	1366		015122.6	+362307	7B	1.70 x 0.45	81	14.7	13.75	5121	5307	421	405	428	0.79	0.93	0.84	3.9	10.10	8.79	0	2	1
	1376	N 721	015145.9	+390813	5B	1.80 x 1.00	58	13.8	12.90	5594	5787	302		355	4.32	4.40	3.40		10.51	9.54	1	1	2
522-058	1385		015152.6	+364045	3B	0.80 x 0.60	43	14.2	13.61	5529	5715						1.64		10.22		0	0	1
522-061			015201.2	+363730	5	0.60 x 0.60	0	15.2	15.03	4919	5105	516	477		0.72	0.78	0.95	2.9	9.55	8.68	0	2	1

© American Astronomical Society • Provided by the NASA Astrophysics Data System

1993AJ....105.1251W

TABLE 2. (continued)

CGCG	UGC	NGC/IC	RA	Dec	T	a x b	i	m_z	m_c	V_{sun}	V_o	W_1	W_2	W_c	F_{obs}	F_c	rms	snr	log L	log M_H	I	Q	Ref
522-062			015204.3	+364036	5B	0.90 x 0.50	58	15.2	14.89	5621	5807	198	191	233	1.79	1.96	1.73	6.2	9.72	9.19	0	1	1
522-063	1387		015213.9	+360057	8	1.10 x 0.90	36	15.4	15.37	4532	4717	231	197	394	3.24	3.67	2.46	7.3	9.35	9.28	0	3	1
522-064	1388	I 171	015214.5	+350210	12	2.50 x 2.20	29	13.8	13.09	5362	5545						1.00		10.40		0	0	1
522-065			015217.8	+351246	3	1.00 x 0.20	90	15.6	15.25	5706	5889	458	420	449	1.39	1.52	0.70	7.7	9.59	9.09	0	1	1
522-069	1398		015300.8	+365300	7	1.40 x 1.20	32	14.9	14.66	5217	5402	153	134	290	1.04	1.24	1.59	5.5	9.75	8.93	0	3	1
522-071	1400		015307.8	+355308	5	2.50 x 0.35	90	13.8	12.09	5336	5518	998	962	980	1.07	1.37	0.68	3.8	10.79	8.99	0	2	1*
522-073	1404		015326.2	+365816	5B	1.40 x 0.60	67	15.6	15.40	4474	4659	234	215	253	2.95	3.37	1.97	7.8	9.32	9.24	0	1	1
522-078	1411	N 735	015342.3	+335600	5	1.80 x 0.80	66	13.9	12.88	4632	4809	462	432	504	13.17	15.85	2.34	18.6	10.36	9.94	0	1	1
522-079			015343.4	+352051	7	0.80 x 0.50	52	15.3	14.99	5229	5411	220	212	279	1.91	2.08	1.85	5.5	9.62	9.16	0	1	1
522-080	1415		015346.5	+360817	2	1.10 x 0.25	87	14.5	13.78	4796	4980						0.89		10.03		0	0	1
522-081	1416		015348.0	+363840	12	1.30 x 0.70	59	14.9	14.38	5465	5649	380	366	441	1.81	2.06	1.54	6.3	9.90	9.19	0	1	1
522-086	1437	N 753	015445.4	+354021	7	3.30 x 2.10	51	12.6	11.66	4901	5082	333	314	429	23.77	39.76	3.33	31.5	10.89	10.38	0	1	1
522-094	1456	I 178	015556.7	+362558	4	1.40 x 0.90	51	14.0	13.22	4845	5028	284	264	362	1.34	1.56	1.04	6.8	10.26	8.97	0	1	1
522-096	1459		015609.2	+354914	7	1.60 x 0.20	90	15.4	14.45	5469	5649	432	385	425	1.53	1.76	1.11	6.8	9.87	9.12	0	1	1
522-099			015700.6	+362058	12	0.55 x 0.35	51	15.4	15.11	5343	5525	221	163	281	2.12	2.26	1.51	8.5	9.59	9.21	0	3	1
	1472		015702.2	+340600	9	1.30 x 1.20	23	18.0	17.79	4849	5026	146	131		3.29	3.88	2.43	12.5	8.43	9.36	0	1	1
522-100	1474		015712.5	+372137	8B	1.60 x 1.20	43	15.0	14.79	4045	4230	174	160	260	3.03	3.68	2.71	7.7	9.48	9.19	0	1	1
522-102	1493		015755.9	+375815	4B	2.30 x 0.80	73	14.0	13.00	4104	4288	279	262	289	1.27	1.62	2.14	3.9	10.21	8.85	0	3	1
	1535		020012.8	+360427	9	1.10 x 0.90	36	17.0	16.77	4321	4501	80	52	136	3.19	3.61	3.75	15.9	8.75	9.24	0	3	1
522-105	1541	N 797	020027.9	+375241	3	1.90 x 1.40	44	13.1	12.28	5654	5836	448	410	637	6.14	7.83	3.13	7.1	10.77	9.80	0	1	1
522-106	1550	N 801	020044.9	+380111	7	3.30 x 0.70	90	13.5	12.02	5766	5951	465		465	17.80	18.64	4.70		10.89	10.19	1	1	2
	1568		020151.2	+352446	8	1.10 x 1.10	0	17.0	16.72	5566	5742	134	103		0.93	1.07	1.54	7.2	8.98	8.92	0	3	1
522-108			020218.8	+343313	12	0.90 x 0.25	80	15.4	14.72	4412	4585	367	365	372	0.95	1.03	1.00	3.8	9.58	8.71	0	3	1
522-111	1581		020236.0	+343836	7	1.80 x 0.80	66	15.2	14.74	4412	4585	352	334	388	11.79	14.22	1.89	26.2	9.57	9.85	0	1	1
522-116	1633	N 818	020542.7	+383222	6B	3.50 x 1.40	69	12.7	11.61	4246	4427	467	452	500	11.88	18.79	3.56	10.8	10.80	9.94	0	1	1
	1642		020611.5	+365827	12	1.40 x 0.10	90	17.0	15.48	4639	4815	186	165	183	4.05	4.57	3.41	8.5	9.32	9.40	0	1	1
	1642b		020611.5	+365827						4193	4369	340	292		3.50	3.68	2.17	5.7		9.22	0	3	1*
	1650		020626.1	+370120	7	2.20 x 0.10	90	17.0	15.32	4586	4764	248	233	244	4.21	5.19	2.15	10.9	9.38	9.44	0	1	1
	1655	N 828	020707.0	+385723	10	3.50 x 2.70	41	13.0	12.30	5335	5515	464		707	12.73	13.78	2.63		10.71	10.00	1	1	5
522-131	1676	N 841	020816.9	+371548	4B	2.00 x 1.00	62	12.8	11.82	4543	4720	415	397	467	5.52	6.88	2.86	7.8	10.77	9.56	0	1	1
522-132			020831.6	+343453	7	0.80 x 0.70	30	15.6	15.53	13579	13748	399	333		1.57	1.72	0.94	7.5	10.21	9.89	0	1	1
522-133	1685		020841.5	+334850	4	1.10 x 0.25	87	14.9	14.00	6175	6341	446	432	440	4.50	4.95	1.83	8.4	10.15	9.67	0	1	1
522-140	1721		021132.6	+371033	6B	2.30 x 2.30	0	14.5	14.10	4639	4814	136	113		8.95	13.33	5.16	18.1	9.87	9.86	0	1	1
523-005	1737	N 861	021250.8	+354100	5	1.50 x 0.60	69	14.8	14.01	8199	8368	524	504	551	3.65	4.21	1.41	10.8	10.39	9.84	0	1	1
	1771		021516.3	+373946	8	2.20 x 1.80	36	17.0	16.68	4331	4503	64	53	109	2.90	4.01	7.23	7.8	8.78	9.28	0	3	1
523-014	1772		021524.5	+374740	12	1.10 x 0.50	65	13.7	12.63	5050	5222	433	236	474	3.40	3.77	4.01	4.6	10.53	9.38	0	2	1
523-017	1778		021553.2	+332945	9	1.40 x 1.10	39	15.6	15.59	5034	5195	190	174	300	3.40	4.01	1.04	21.0	9.34	9.41	0	1	1
	1784		021609.2	+362405	9	1.20 x 0.70	55	17.0	16.84	6476	6645	133	119	161	0.58	0.65	1.43	4.6	9.06	8.83	0	2	1
523-019			021618.0	+333447	6	0.90 x 0.30	75	15.6	15.15	8567	8728	421	386	432	2.65	2.88	1.51	7.6	9.97	9.71	0	1	1
523-022	1787		021635.5	+374223	7	1.40 x 0.50	73	14.7	13.89	6421	6593	423	407	443	6.33	7.21	6.64	4.2	10.23	9.87	0	3	1
523-027	1804		021753.9	+382545	9	1.70 x 0.80	64	15.5	15.49	5188	5361	210		235	2.96	3.00	4.55		9.41	9.31	1	2	2
523-028	1810		021824.3	+390850	5	2.10 x 1.40	49	13.7	12.83	7531	7707	613		800	15.61	16.03	4.40		10.79	10.35	1	3	2
523-030	1826		021905.5	+334307	12B	1.20 x 0.35	78	14.6	13.49	5008	5167	215	187	218	4.59	5.10	1.50	19.8	10.18	9.51	0	1	1
523-031	1829		021923.4	+333126	9	1.10 x 0.80	44	15.7	15.69	3664	3823	105	81	152	1.66	1.87	1.97	10.4	9.04	8.81	0	1	1
523-042	1886		022254.6	+391450	5	4.50 x 2.30	61	13.1	12.09	4856	5029	496		564	16.60	18.37	4.30		10.72	10.04	1	1	2
523-043	1910		022355.9	+345733	12	2.30 x 0.60	81	14.8	13.86	5128	5286	391	325	393	7.09	8.94	1.44	20.2	10.05	9.77	0	1	1
523-046	1919		022436.0	+355540	5B	1.60 x 1.10	48	15.0	14.63	10749	10910	334	319	442	2.57	3.09	2.48	5.4	10.37	9.94	0	1	1
	1959		022609.3	+341833	9	1.20 x 0.80	49	18.0	17.77	3552	3709	160	71	214	0.85	0.97	1.20	7.7	8.18	8.50	0	3	1
523-051	1976		022719.6	+350616	5	1.70 x 0.80	64	15.0	14.47	9117	9276	497	464	543	6.04	7.19	2.26	7.4	10.29	10.16	0	1	1
	1983	N 949	022745.1	+365453	7	3.60 x 2.30	51	12.0	11.15	612	773	194		254		16.90	4.00		9.46	8.38	B	1	3
	1993		022833.5	+390933	7	2.40 x 0.60	83	14.3	13.15	8018	8187	496		497	6.72	6.89	3.18		10.72	10.04	1	1	2
523-063	2054		023131.6	+334327	8	1.70 x 1.00	55	15.3	15.07	4437	4587	274	258	336	2.96	3.58	2.16	8.4	9.44	9.25	0	1	1
	2055		023133.1	+365520	8	1.40 x 1.00	45	18.0	17.66	3774	3933	192	179	272	5.01	5.87	3.73	9.2	8.27	9.33	0	1	1
523-064			023137.1	+344013	6	0.90 x 0.30	75	15.0	14.19	3762	3915	262	226	273	9.04	9.82	2.98	14.6	9.66	9.55	0	1	1
523-066	2065		023217.4	+371607	12	1.70 x 1.70	0	14.6	14.29	3890	4051	121	97		7.66	9.87	5.25	15.3	9.65	9.58	0	1	1*
523-067	2067		023224.0	+371813	4	2.50 x 0.50	90	14.8	13.90	3861	4022	259	99	256	5.76	7.40	2.64	16.9	9.80	9.45	0	5	1*
523-069	2077		023309.0	+342240	7	1.10 x 0.90	36	15.5	15.44	11759	11911	243	225	404	2.10	2.38	1.55	8.8	10.12	9.90	0	1	1
523-073	2090		023335.2	+342333	5	1.10 x 1.00	25	15.4	15.33	9478	9629	399	379		5.35	6.10	2.08	10.2	9.98	10.13	0	1	1
523-074	2094		023347.5	+355341	7B	2.30 x 2.20	17	13.8	13.10	5132	5286	282	259		7.20	10.58	2.89	15.2	10.35	9.84	0	1	1
523-076	2105		023437.7	+341259	3B	1.60 x 1.30	37	13.9	13.28	4921	5072	294	255	483	2.79	3.41	1.01	9.2	10.25	9.32	0	1	1

© American Astronomical Society • Provided by the NASA Astrophysics Data System

1993AJ....105.1251W

TABLE 2. (continued)

CGCG	UGC	NGC/IC	RA	Dec	T	a x b	i	m_z	m_c	V_{sun}	V_o	W_1	W_2	W_c	F_{obs}	F_c	rms	snr	log L	log M_H	I	Q	Ref
523-077	2109		023456.3	+340131	7	1.90 x 1.70	27	14.5	14.03	3677	3827	177	161		5.19	6.84	2.16	18.6	9.70	9.37	0	1	1
523-079	2133	N1002	023552.3	+342433	5B	1.60 x 1.00	52	14.0	13.25	4720	4870	386	374	486	1.18	1.41	1.35	4.5	10.22	8.90	0	3	1
523-080			023553.4	+352311	5	0.70 x 0.25	73	15.5	14.89	9243	9396	336	290	345	1.91	2.05	1.22	8.9	10.14	9.63	0	3	1
523-081	2143		023632.5	+355201	10	0.55 x 0.55	0	14.0	13.45	2754	2906	127	97		4.34	4.66	4.53	11.5	9.69	8.97	0	1	1
523-087	2166		023805.4	+353840	7	1.40 x 0.70	62	15.7	15.60	3139	3290	156	141	179	2.63	3.02	1.55	12.3	8.94	8.89	0	1	1
524-002	2179		023929.4	+345933	7B	1.70 x 1.70	0	15.1	15.05	3554	3701	127	111		2.22	2.86	1.42	16.6	9.26	8.97	0	1	1
	2178	N1050	023931.8	+343301	5B	1.80 x 1.20	49	13.5	12.57	3901	4048	283		374	1.37	1.70	1.80		10.33	8.82	0	1	3
524-007	2212		024123.4	+333133	12	1.10 x 0.50	65	15.4	15.02	5327	5470	258	239	282	3.36	3.73	2.21	8.9	9.62	9.42	0	1	1
524-012	2223		024209.0	+345840	7	1.20 x 0.35	78	14.8	13.89	4981	5126	276	251	283	2.71	3.02	1.82	9.1	10.01	9.27	0	1	1
524-015			024331.1	+345000	7	0.70 x 0.70	0	15.2	14.95	14008	14152	225	198		1.50	1.64	1.91	6.1	10.47	9.89	0	1	1
524-022	2274	N1093	024512.3	+341241	12	2.20 x 1.40	51	14.3	13.53	5282	5425	383	369	487	9.69	12.84	1.22		10.21	9.95	0	1	1
524-025	2305		024635.9	+375147	7	1.50 x 1.00	49	15.5	15.38	5408	5559	201	186	267	5.24	6.20	2.99	11.3	9.49	9.66	0	1	1
524-035			025221.5	+360000	7	0.70 x 0.60	32	15.6	15.45	8660	8804	236	192	443	0.80	0.87	1.45	5.6	9.86	9.20	0	3	1
524-036	2392		025242.0	+333400	7	2.00 x 0.50	83	15.0	14.06	1548	1683	168	151	172	5.90	7.17	3.59	14.0	8.98	8.68	0	3	1
	2417		025346.4	+360727	9	1.20 x 1.10	24	18.0	17.55	3643	3786	155	137		4.35	5.04	3.19	10.0	8.28	9.23	0	1	1
524-037	2435		025457.3	+350333	7	2.50 x 2.00	38	14.6	13.93	4850	4989	250	231	408	8.35	12.28	3.07	15.1	9.97	9.86	0	1	1
524-038	2448		025600.0	+334250	10	1.30 x 0.40	77	15.6	15.51	3891	4023	126	83	129	6.22	6.98	3.58	20.0	9.15	9.43	0	3	1
524-039			025613.6	+335447	7	0.75 x 0.50	49	15.7	15.54	11848	11980	356	288	463	1.48	1.60	1.14	5.4	10.09	9.73	0	3	1
524-042	2461		025717.2	+335230	7	1.20 x 0.50	68	15.7	15.26	6807	6938	325	306	350	1.80	2.01	1.28	7.1	9.73	9.36	0	1	1
	2466		025729.4	+352600	9	1.70 x 0.90	60	16.5	16.03	4980	5117	287	270	334	1.79	2.15	1.15	8.6	9.15	9.12	0	1	1
524-043	2465		025731.1	+345827	3	1.30 x 0.35	81	14.7	13.73	5078	5212	413	148	412	1.86	2.08	1.00	9.9	10.09	9.13	0	3	1*
524-045	2487	N1167	025835.3	+350031	1	3.30 x 2.30	47	14.0	13.02	4945	5081	487	452	657	5.59	9.51	1.82	12.4	10.35	9.76	0	1	1
524-046	2491		025846.6	+353213	3B	2.20 x 1.80	36	14.8	14.13	4875	5011	190	173	316	3.93	5.42	1.90	16.3	9.89	9.51	0	1	1
524-048	2494		025856.2	+355410	12	1.10 x 0.50	65	14.7	13.60	7894	8030	600	565	651	3.49	3.87	1.69	6.2	10.52	9.77	0	1	1
524-049	2526		030234.4	+363542	5	4.50 x 0.80	90	13.5	11.45	4962	5099	600	558	591	6.85	11.69	1.83	13.0	10.98	9.86	0	1	1
524-050		I1874	030313.1	+354927	2B	0.90 x 0.60	49	14.8	14.16	4924	5057	370	346	481	1.07	1.17	1.11	4.5	9.89	8.85	0	3	1
524-051	2540		030352.4	+355836	4	1.90 x 0.20	90	15.7	14.56	3929	4062	428	415	422	6.47	7.70	2.32	8.9	9.54	9.48	0	1	1
	2541		030408.6	+340926	12	1.20 x 0.80	49	17.0	16.17	11479	11608	246	222	317	2.05	2.33	1.37	8.9	9.81	9.87	0	1	1
524-052	2543		030411.7	+374847	12	2.10 x 0.70	75	14.9	13.83	5251	5390	336	324	346	4.03	4.99	3.33	5.9	10.08	9.53	0	1	1
524-055	2548	N1207	030503.0	+381126	5	2.80 x 1.80	51	13.7	12.44	4800	4941	437	378	560	4.33	6.48	1.64	8.4	10.56	9.57	0	1	1*
524-056	2550		030506.0	+361533	7	1.70 x 0.90	60	15.1	14.30	4022	4157	264	235	309	4.87	5.85	3.02	9.0	9.67	9.38	0	1	1
524-058	2557	N1213	030604.1	+382727	8	3.00 x 2.30	41	15.7	15.51	3428	3568	160	142	246	15.01	15.92	5.31	24.9	9.05	9.68	1	1	1
	2566		030706.5	+334104	12	1.10 x 0.70	51	17.0	16.11	12506	12630	290	262	361	2.09	2.34	1.23	11.7	9.91	9.94	0	3	1
	2586	N1233	030919.2	+390750	5	2.30 x 0.90	70	13.9	12.44	4407	4548	497		527	18.68	19.15	8.00	4.2	10.49	9.97	1	1	2
525-007			031047.5	+334653	7B	0.90 x 0.35	70	15.7	15.22	12261	12382	366	342	382	2.29	2.49	1.37	6.4	10.25	9.95	0	1	1
525-008			031106.0	+352110	6	1.00 x 0.15	90	15.6	14.59	5264	5392	299	271	294	2.93	3.20	1.84	8.3	9.77	9.34	0	3	1
525-009	2604		031130.0	+392700	7B	1.60 x 1.20	43	14.8	14.03	4531	4671	309		460	4.32	4.39	5.30	9.7	9.88	9.35	1	1	2
525-011	2610		031148.0	+391100	5	1.20 x 0.50	68	15.7	15.10	5090	5230	279		299	3.44	3.46	2.47	7.9	9.54	9.35	1	1	2
525-010	2609	I 304	031149.1	+374156	5	1.30 x 0.80	53	14.8	13.73	4938	5071	372	320	463	5.41	6.19	2.53	11.5	10.07	9.58	0	3	1
525-016	2623		031319.6	+345247	7B	2.70 x 2.50	23	15.7	15.34	4425	4548	121	107		7.07	11.40	2.69	26.0	9.33	9.75	0	1	1
525-017	2630		031400.0	+365700	6	1.00 x 0.25	83	15.5	14.45	5116	5245	456	439	460	2.67	2.92	1.96	4.6	9.81	9.28	0	3	1
525-018			031410.3	+360126	6	0.60 x 0.60	0	15.7	15.60	5534	5663	251	203		3.79	4.09	2.19	12.0	9.41	9.49	0	1	1
	2633		031412.0	+362310	7	1.60 x 0.20	90	17.0	15.10	5668	5797	545	499	536	3.07	3.53	1.66	7.0	9.63	9.45	0	1	1
	2637		031418.0	+375040	7	1.50 x 0.20	90	17.0	15.19	5126	5258	293	275	289	3.02	3.44	2.69	5.7	9.51	9.35	0	1	1
	2653		031526.2	+372537	7	2.30 x 0.80	73	16.5	15.15	6939	7070	460	428	479	9.12	11.68	2.79	13.9	9.79	10.14	0	1	1
	2678		031722.1	+371900	5B	1.70 x 1.50	29	16.0	15.11	5591	5720	390	372		2.84	3.58	1.75	7.2	9.62	9.44	0	1	1
525-023	2685		031738.4	+380423	5B	2.20 x 1.70	41	14.8	13.79	5044	5176	237	218	362	9.97	13.61	6.54	9.7	10.06	9.93	0	1	1
525-024			031902.8	+361640	12	0.55 x 0.55	0	15.6	15.42	4843	4968	146	113		1.59	1.71	2.22	6.7	9.37	9.00	0	3	1
525-025	2702		031940.9	+365127	12	3.00 x 2.80	22	15.5	15.07	4787	4912	401	385		7.01	12.27	2.70	11.8	9.50	9.84	0	1	1
	2707		032028.5	+365150	8	1.40 x 0.70	62	18.0	16.93	4883	5007	164	146	187	2.33	2.68	2.08	10.7	8.78	9.20	0	1	1*
525-027	2706		032030.6	+364440	8	1.20 x 1.20	0	15.7	15.43	4721	4845	225	206		4.12	4.81	2.70	8.6	9.34	9.43	0	1	1
525-029	2709		032039.6	+383000	5	3.50 x 1.30	72	14.8	13.62	5146	5276	390	363	409	14.13	14.94	3.99	14.4	10.14	9.99	1	1	2
	2750		032533.9	+362428	6	1.60 x 0.15	90	16.5	14.59	4859	4980	563	484	554	2.02	2.32	1.13	7.9	9.70	9.13	0	2	1
525-040	2770		032807.1	+351753	5B	1.70 x 1.50	29	14.9	13.99	4479	4594	142	128		3.57	4.50	2.07	13.9	9.88	9.35	0	1	1
	2778		032938.3	+360300	5B	1.10 x 0.90	36	16.5	15.62	5992	6110	304	222	510	1.08	1.22	3.03	4.5	9.47	9.03	0	2	1
	2780		033000.7	+360100	12	1.80 x 1.70	20	16.5	15.71	4513	4630	161	152		2.76	3.59	2.07	11.0	9.20	9.26	0	1	1
526-003	2810		033648.0	+392700	7	1.20 x 1.10	24	15.0	14.10	6500	6623	293			3.20	3.24	1.62		10.15	9.53	1	1	2
	2817		033818.0	+370200	12	2.30 x 0.80	73	17.0	15.35	5755	5870	436	132	451	3.41	4.35	2.25	7.9	9.55	9.55	0	3	1
526-008	2857		034340.6	+382950	5B	1.50 x 1.10	44	15.0	13.63	6444	6559	392	340	560	3.63	4.32	2.75	5.9	10.33	9.64	0	3	1
	2861		034424.0	+391200	5	2.30 x 1.30	57	16.0	14.31	6394	6511	541		640	27.40	28.21	6.60		10.05	10.45	1	1	2

© American Astronomical Society • Provided by the NASA Astrophysics Data System

1993AJ....105.1251W

TABLE 2. (continued)

CGCG	UGC	NGC/IC	RA	Dec	T	a x b	i	m_z	m_c	V_{sun}	V_o	W_1	W_2	W_c	F_{obs}	F_c	rms	snr	log L	log M_H	I	Q	Ref
	2875		034717.4	+362307	12	1.10 x 0.30	80	16.5	14.76	5767	5872	297	47	299	2.69	2.96	1.28	17.0	9.78	9.38	0	1	1
	2877		034747.8	+364453	9	1.60 x 0.90	57	17.0	15.65	3816	3921	103	89	124	1.51	1.79	1.99	8.8	9.07	8.81	0	1	1
	2882		034923.5	+343207	8	1.80 x 0.70	70	17.0	15.71	4268	4365	216	197	231	4.05	4.85	3.13		9.15	9.34	0	1	1
526-012	2885		034948.6	+352633	7	5.50 x 2.50	65	14.4	12.74	5803	5903	537		593		27.50			10.60	10.35	B	1	4
	2886		034950.7	+344836	8	1.70 x 1.30	41	18.0	17.00	5387	5483	138	126	210	1.46	1.81	1.63	8.6	8.83	9.11	0	1	1*
526-013	2889		035020.8	+370700	6B	1.60 x 0.80	62	15.7	14.49	5580	5687	352	324	399	3.50	4.13	1.81	8.8	9.86	9.50	0	3	1
	2893		035100.0	+362150	7B	1.20 x 1.00	35	17.0	15.65	5833	5936	172	152	303	3.04	3.50	2.05	11.6	9.44	9.46	0	1	1
	2901		035326.0	+344300	12	1.10 x 1.10	0	16.0	14.98	8452	8546	234	216		2.73	3.14	1.42	12.9	10.02	9.73	0	1	1
526-016	2920		035734.3	+345227	7	2.30 x 0.40	90	15.3	13.64	4158	4249	376	368	375	8.55	10.74	2.30	13.4	9.95	9.66	0	1	1
	2932		035936.3	+334360	8	1.10 x 1.00	25	18.0	16.94	4880	4966	211	201		2.68	3.06	1.56	12.4	8.77	9.25	0	1	1
526-017	2945		040124.0	+334000	2	1.50 x 1.10	44	15.2	14.26	5230	5315	234	208	332	6.52	7.76	1.19	41.4	9.90	9.71	0	1	1
	2959		040353.2	+341803	10	1.40 x 1.20	32	16.0	14.59	5546	5632	99		186	3.67	4.36	4.75		9.81	9.51	0	1	6
	2991		041042.3	+364320	5B	2.20 x 1.70	41	16.5	14.46	6032	6121	257	232	391	7.11	9.71	3.58	11.6	9.94	9.93	0	1	1
	3007		041516.3	+333920	7	1.30 x 1.10	33	17.0	15.63	5631	5706	97		178	4.80	5.61	2.91	20.0	9.41	9.63	0	3	6
	3028		042119.9	+334540	12	1.70 x 0.80	64	16.0	14.02	5484	5554	452		499	10.68	12.71	1.74	19.0	10.03	9.97	0	1	6

Notes to Table 2

514-012 = N7263 : observed on CGCG position, as given.
U12008 : pointing and flux calibration uncertain.
514-020 = U12012 : pair with -019 at 3.9', 211; no evidence of blend.
514-039 = U12051 : highly asymm, poor s/n; vel, width, flux uncertain.
514-071 = U12120 = N7342 : as above.
514-090 = U12137 : flux calibration uncertain.
516-002 = U12474 : signal identification uncertain; signal could be much broader (~ 650 km/s), and centered near 4900 km/s.
517-014 : 80 mJy continuum source within beam; absorption feature probably real (no obvious optical feature in off position at $00^h05^m23^s$, same dec; check for HI emission in off field not done).
519-007 : interference makes signal identification quite doubtful.
519-021 = U480 : probable blend with -022 at 1.4'.
520-023 = U755 : poor flux calibration.
520-026 = U758 : as above.
520-036 = U831 : as above.
521-017 : confused with -018 at 2.5'; parms. v. uncertain.
521-018 = U944 = N512 : at 2.5' from -017; no evidence of disturbance in this spectrum.
U1316 : pair with 522-023 at 1.5'.
522-071 = U1400 : parms. v. uncertain; other candidate for signal at ~ 4025 km/s.
U1642b : in spectrum on U1642, two well separate features appear; we attribute that at 4639 km/s to U1642 because of its symmetry and resemblance of rotating disk; other feature might be associated with extended emission from one of the companions of U1642, located respectively at 4.3' and 3.8'.
523-067 = U2067 : pair with -066 at 2.5'; blend; parms. quite uncertain.
524-043 = U2465 : asymm. profile: poor pointing?
524-055 = U2548 : poor flux calibration.
U2707 : previously reported velocity (Beers et al. 1986) of 3405 km/s is incorrect.
U2886 : both U2886 and U2887 (1.1x1.0, dwarf, m=18) within the beam (sep. 1'); unable to discern two separate features, assignment of full flux to U2886 arbitrary.

Column (23)—Quality code for H I detection: 1—high quality detection, 2—marginal or poor detection, 3—flux and velocity ok, but profile unsuitable for use in T–F relation, 4—H I seen in absorption, 5—confused with neighbor.

Column (24)—Reference code for H I data. The H I data reported here come from one of the following sources: 1—This survey, 2—Northern Pisces–Perseus region (Haynes *et al.* 1988), 3—Isolated galaxy survey (HG84), 4—Survey of large angular diameter galaxies (Hewitt *et al.* 1983), 5—Magri (1990), and 6—Sc galaxy survey (in preparation). When followed by a '*', see notes at the end of the table.

2.3 The Overall Redshift Sample

In the northern region of the PP supercluster referred to as the "northern box," bounded by $22^h < \text{R.A.} < 4^h, +20°$ $< \text{Dec.} < +50°$, our compilation now includes 3311 galaxies of known redshift, of which 2891 are at $V_{\text{Sun}} < 12\,000$ km s^{-1}. Within that region, there are 2888 CGCG galaxies (catalogued magnitudes 15.7 or brighter); of those, 2340 have measured redshifts. Two thousand and eighteen galaxies have 21 cm measurements, of which 1798 have been presented by us. Our contribution in this region to the optical redshift data base amounts to 503 galaxies, including those given here and others by Sakai *et al.* (1993). The sky distribution of galaxies with heliocentric radial velocities smaller than 12 000 km s^{-1} in the northern box are displayed in Fig. 1. The region includes the vast majority of spectroscopic measurements reported in Tables 1 and 2.

The new data reported here make a significant contribution to this overall sample. This is because they probe the high density structure of the PP ridge and we use them in the study given in the remaining sections.

Strictly referring to the declination range between 33.5 and 39.5 degrees, Figs. 2 and 3 illustrate the degree of completeness of the redshift survey in that region. Figure 2 displays the number of known redshifts, as a function of CGCG magnitude, $n(m)$, and the completeness fraction

© American Astronomical Society • Provided by the NASA Astrophysics Data System

1993AJ....105.1251W

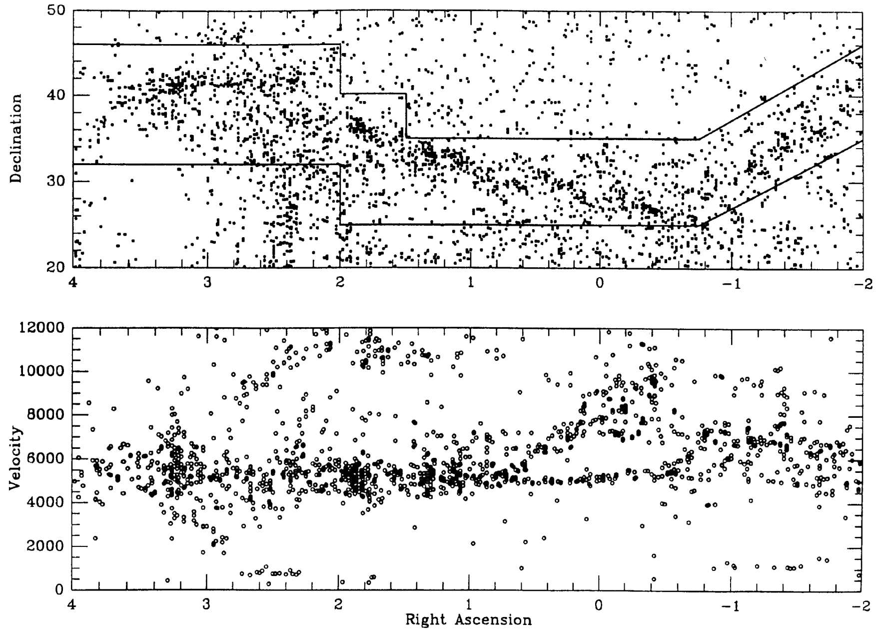

FIG. 1. Separate two-dimensional views of galaxy distribution in the northern PP box. The upper panel shows the sky distribution of all galaxies in the overall northern box sample. The region believed to contain the PP main ridge is outlined. The lower panel shows the two dimensional R.A.–V_0 for galaxies in the ridge region highlighted in the upper panel.

$c(m)$, defined as the ratio of $n(m)$ to that of catalogued objects in the given magnitude bin. Overall completion is better than 75% except for the last two bins, i.e., for galaxies fainter than 15.5. Figure 3 illustrates completion as a function of major angular (blue) diameter of the galaxy. The solid histogram includes galaxies of known redshift, while the dotted one displays the size distribution of CGCG galaxies. The latter is a subset of the former for sizes larger than 1′, as many low surface brightness UGC galaxies, fainter than 15.7, have measured redshifts as well.

3. THE MAIN RIDGE OF THE PISCES–PERSEUS SUPERCLUSTER

With the availability of this enlarged redshift compilation as well as positional information, it is now possible to obtain a detailed view of the galaxy distribution in the main ridge of the supercluster. In this section, we examine evidence that the northern supercluster is dominated by a high density linear ridge. Note however, that the southern extension of the supercluster appears quite different in both sky and cone diagram projections (Haynes & Giovanelli 1988), and thus we are, if anything, only examining part of the overall connective structure in this large portion of the sky.

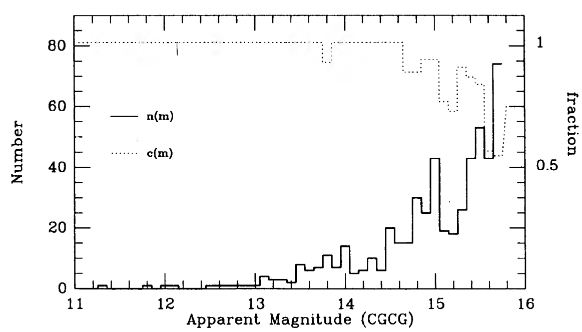

FIG. 2. Magnitude distribution of galaxies with known redshift in the 33.5° to 39.5° declination strip of the PPS region (solid line) and completeness fraction (dotted line). The completeness fraction is the ratio, for each magnitude bin, of the number of galaxies of known redshift to that of galaxies catalogued in the CGCG.

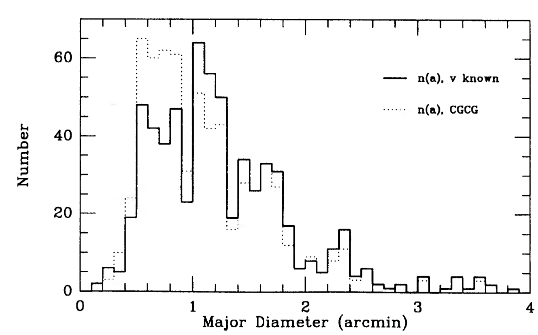

FIG. 3. Major blue angular diameter distribution of galaxies of known redshift (solid line), and distribution of those listed in the CGCG (dotted line).

© American Astronomical Society • Provided by the NASA Astrophysics Data System

1993AJ....105.1251W

3.1 Confinement on the Plane of the Sky

In GHC, we examined the large-scale galaxy distribution in PP using a much less complete set of redshift data. In particular, Fig. 1 of GHC presents a shade intensity diagram of the overall PP region extending across all fifty degrees of declination. Here we consider only the northern portion and the reader is referred to GHC and Haynes & Giovanelli (1988) for the regionwide picture. Similar to Fig. 4 of GHC, Fig. 1 shows separate two-dimensional slices to establish the identification of the PP ridge in better detail. In the upper panel, the sky distributions within the northern box of all 3517 galaxies (of magnitude 15.7 or brighter or major angular diameter larger than 1′) in the current sample, including galaxies without measured redshifts is illustrated. Individual galaxy locations are marked by small squares. The Perseus cluster A426, A262, and the Pisces cluster at (R.A.,Dec.)$=01^h04^m$, $+32°$ are evident. Too poor to meet Abell's (1958) richness criteria, the Pisces clusters extend over the center of the main ridge and include the concentrations of galaxies around NGC 383 and NGC 508 in CGCG fields 520–521. Note that galactic obscuration becomes a significant problem in the northern and eastern portions of the map (cf. Fig. 2 of GHC).

The region of highest density extracted from the complete surface density map as illustrated in Fig. 1 of GHC is outlined in Fig. 1. This portion of the sky will be referred to as the "ridge region." Within this region, there are 1631 galaxies with known redshift $V_0 < 12\,000$ km s^{-1}. In the lower panel, the two-dimensional slice in right ascension and velocity is shown only for the objects in the ridge region. A426 is the prominent vertical structure seen at R.A.$=3^h12^m$, and the other clusters are apparent by the flaring of the velocity dispersion at the location of the higher density region also seen in the upper panel. With $V_0=9000$ km s^{-1} (Struble & Rood 1987), A2666 is also visible at R.A.$=23^h48^m$. The structure in the velocity domain, and in particular, the occasional velocity crowding into narrow lanes will be discussed further in Sec. *2.2*.

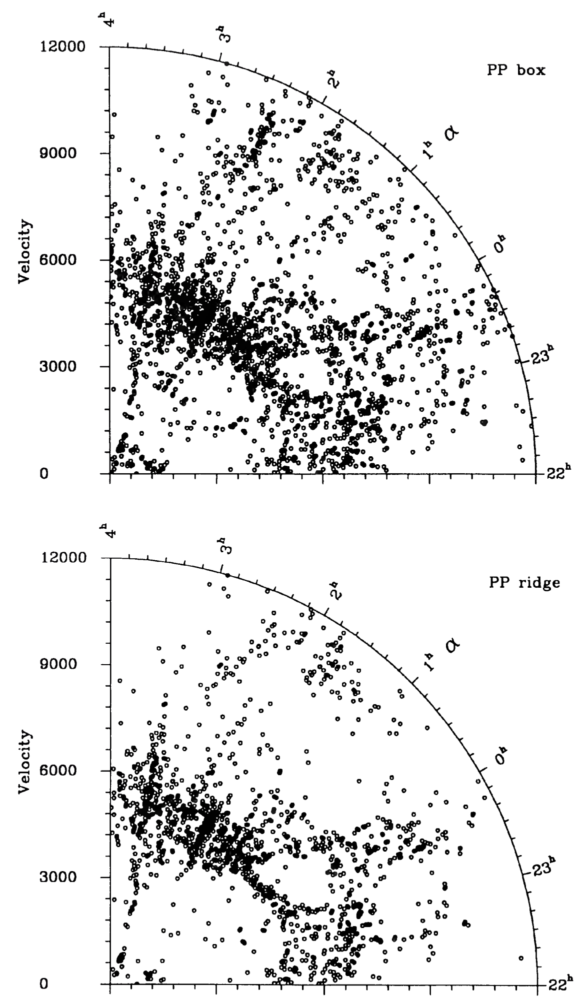

FIG. 4. Velocity cone diagrams with Right Ascension as the angular coordinate with no correction for declination squeezing. The upper panel shows the distribution of all 2891 galaxies with measured redshifts less than 12 000 km s^{-1}, while the lower one includes only the 1631 that lie within the boundaries of the ridge illustrated in Fig. 1.

3.2 Confinement in Velocity

Confining the cluster in the sky direction, we can examine the restriction into a narrow range of velocity space. Figure 4 shows cone diagrams with R.A. as the angular coordinate for the two samples, the northern box (upper panel) and the ridge (lower panel). All galaxies, including objects fainter than $m=15.7$, are included. As in the lower portion of Fig. 1, Fig. 4 well illustrates the basic structure of the PP region: a large overdensity is seen in the velocity range $4500 < V_0 < 6500$ km s^{-1}. A426 is the "finger of God" pointing toward the origin at R.A.$=3^h12^m$. The eastern ridge is characterized by a typical 1-d velocity dispersion about the mean of about 350–500 km s^{-1}, as will be quantified below. If interpreted purely as a spread in the distances to such objects, the corresponding depth of the ridge is about 7–10 h^{-1} Mpc. Of comparable importance is the fact that the foreground is virtually empty of galaxies across almost the entire region. The PP foreground void and its possible connection to the Local Supercluster have been discussed previously (Haynes & Giovanelli 1986). An unsuccessful search for H I rich dwarfs within the void was conducted by Eder *et al.* (1989). As noted by Haynes & Giovanelli (1988), the foreground void can be traced over the entire 50 degree declination range and is thus not spherical. Similar geometry is noted for the void in front of the Hercules supercluster (Freudling 1990). A smaller background hole is evident in Fig. 4, at R.A.$=0^h$, just where the major ridge appears to split into two narrower segments, one extending toward the background and one nearly perpendicular to the line of sight.

One of the most striking features of the PP ridge is its near-perfect orientation at constant redshift from us. Figure 5 attempts to quantify the confinement of the main ridge in both spatial and velocity coordinates. For narrow bins of right ascension within the area outlined in Fig. 1, the right panels show the mean values and their standard deviations of the velocity and declination distributions.

© American Astronomical Society • Provided by the NASA Astrophysics Data System

1993AJ....105.1251W

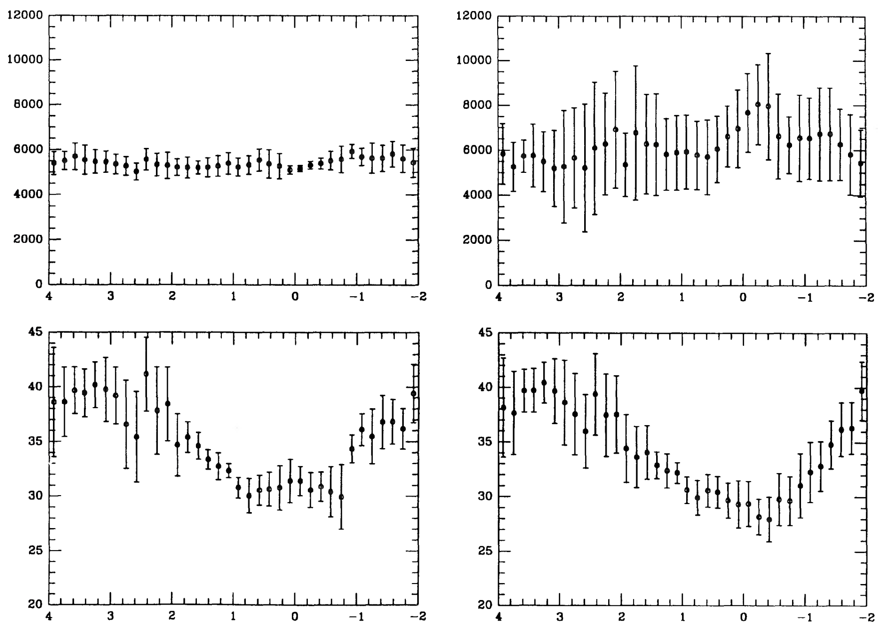

FIG. 5. Mean values and standard deviations of velocity (upper panels) and declination (lower panels) for galaxies in bins of Right Ascension in the ridge region. The right panels show galaxies of all velocity, while the ridge membership criterion $4500 < V_0 < 6500$ km s^{-1} has been used in constructing the left panel.

The left panels show similar distributions but only for galaxies with $4500 < V_0 < 6500$ km s^{-1}. This figure serves to quantify the qualitative impressions given in Figs. 1 and 4. Comparison of the left and right panels is necessary because of the uncertainty in interpreting dispersion as depth in the redshift dimension. Examination of Fig. 5 along with histograms of the velocity distribution in each bin allows the best attempt to delineate the ridge. Where the main clusters are present, the spread in velocity is clearly larger than that indicated in the left hand panel, but in regions of only moderate density, the supercluster ridge is characterized by a typical velocity dispersion in the radial direction of 300–500 km s^{-1} as noted also in Figs. 1 and 4.

In the narrow lane running between R. A. $=23^{\rm h}40^{\rm m}$ and R.A. $=0^{\rm h}15^{\rm m}$, a length of about $9h^{-1}$ Mpc, it lowers to a minimum of only 125 km s^{-1}. Since the dispersion around the velocity mean is so small, and $\langle V \rangle \simeq 5200$ km s^{-1}, the apparent narrowness of lane in velocity is not an artifact of our redshift boundaries for ridge membership but reflects either a true thinness in the redshift dimension or an illusory thinness resulting from perversely tuned infall of galaxies in a broader lane towards a linear structure at its mean distance.

The lane is seen in this diagram to show a decrease in mean velocity of about 220 km s^{-1} from west to east. In the same region, the breadth of the ridge in the declination direction has a width of about 4.2 degrees. Corresponding variations in the distributions are seen in the portions to the east where the declination distribution flairs in the neighborhood of A262 at lower declinations and A347 to the north.

The mean degree of overdensity within the surveyed region can be estimated by comparing the observed redshift distribution to that expected from a homogeneously distributed sample, which would be characterized by some "universal" luminosity function. While the issue of whether a universal luminosity function exists may be open to question, the averaging over the sky coordinates is such to minimize the relevance of that issue vis-a-vis the results discussed here. The scaling of the luminosity function can be obtained by the mean number of galaxies within a distance much larger than that which characterizes the redshift domain of the supercluster. Both the northern box region and the PP ridge exhibit strong clustering over the velocity window $4000 < V_0 < 6000$ km s^{-1}; over that range, and integrated over the whole sky coordinates of the two regions as described above, the northern box and the PP ridge yield overdensities on the order of, respectively, at least 4 and 6.

3.3 Distribution of Groups

Another way to trace the large-scale structure along the ridge is to identify concentrations in the galaxy distribution in three dimensions. As discussed by Haynes & Giovanelli (1991), both visual and automated techniques of cluster analysis can be employed to give the best understanding of structure. Numerical algorithms for identifying clustering in the true galaxy distribution are complicated by the realities that all observed separations are projections and local deviations from Hubble flow are significant on small scales in the vicinity of groups and clusters, and perhaps on large scales as well. The PP ridge is a region of high density where perturbations in the underlying matter distribution are likely to be significant if light traces mass. With the caveat that we are not yet able to interpret the velocity field

© American Astronomical Society • Provided by the NASA Astrophysics Data System

1993AJ....105.1251W

well, we have applied a group-finding algorithm to the objects located within the PP box. The algorithm is based on the percolation technique described by Huchra & Geller (1982) and examines the separation among objects in the spatial and velocity dimensions separately. In attempting to identify groups, we checked the fields of all galaxies, searching for companions in both sky coordinates and redshift. Cutoff values in linear separation for potential partners are allowed to increase with increasing redshift in order to account for Malmquist bias. As discussed in Haynes & Giovanelli (1991), cutoff values in redshift and magnitude must be imposed on the sample in order to use the method properly to give quantitatively meaningful results and a fiducial redshift must be chosen where all galaxies are believed to be counted in defining the density contrast. As in the earlier paper and following Huchra & Geller (1982), we define the cutoff in linear separation for a density contrast of 20 at a fiducial redshift of $V_F \simeq 1000$ km s^{-1} to be 0.5 Mpc. We also required the grouped pairs to be separated in the radial velocity coordinate by less than 600 km s^{-1}.

Note that the application of this group-finding algorithm requires accepting that a mean density can be characterized. In spite of this uncertainty, we can nonetheless examine densities relative to the mean density *of this volume*. Additionally, Gourgoulhon *et al.* (1992) have discussed a distance dependent bias that needs to be taken into consideration in the group identification process; since we will be interested only in structures within the supercluster, i.e., all at roughly the same distance from us, we have not introduced their correction. Our purpose is to obtain a qualitative impression of the supercluster structure, rather than to claim group membership in this volume, where velocity dispersion and peculiar motions might introduce considerable scatter in group assignments. A more detailed examination of the true three-dimensional structure requires a more sophisticated attempt to recover the true density field both from studies of the apparent distribution of galaxies and from the measurement of peculiar motions with the aid of redshift-independent distances. Although we are presently pursuing these studies, here we mean to provide a more general discussion of how rather fortuitous aspects of this supercluster influence our initial impressions.

Figure 6 displays the distribution of groups in the northern ridge. Each panel shows the location of galaxies meeting certain criteria of local density. From top to bottom: galaxies found to be isolated at contrast = 20 and members of groups found at contrast = 30 000, 300, and 20 times the mean density. Galaxies in the same grouping are marked by the same symbol type; note that because of the large number of groups, symbols must be repeated, but with a regularity of pattern with increasing group mean right ascension. Because groups often fragment into separate subconcentrations as contrast is increased, it is not possible to track a galaxy from one panel to the other with the same symbolic marking. Hence galaxies do not have the same representation in successive panels.

The bottom panel shows the locations of all galaxies

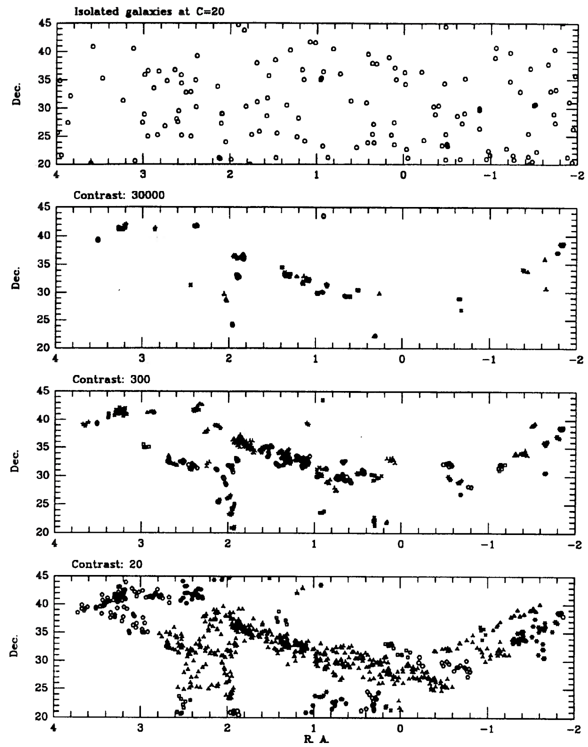

FIG. 6. The sky distribution of galaxies selected by certain density criteria. The uppermost panel shows the distribution of 145 isolated galaxies, i.e., galaxies found not to have any companions at a contrast of 20. The second and third panels from the top display galaxies found in groups at density contrast of, respectively, 30 000 and 300. The bottom panel displays galaxies that are members of groups in which the density is 20 times higher than the mean density in the surveyed region.

that the group-finding algorithm identifies as members of groups in which the density is 20 times the mean density. Note that at this low density contrast a single structure extends along the whole supercluster ridge from just east of Abell 262 west to Pegasus and south. Indeed, this single "group" contains 576 galaxies. A second populous structure surrounds the Perseus cluster.

The second panel from the bottom in Fig. 6 displays the galaxies in groups found at a density contrast of 300. Many of the groups are now seen to be separate clumps of the

TABLE 3. Highest density groups in the PP Supercluster.

Name	RA hh mm.m	Dec dd mm	N	$<z>$ kms^{-1}	σ kms^{-1}	r_H Mpc
513-015	22 09.6	38 31	5	5889	240	0.26
N7318	22 33.6	33 42	4	5984	418	0.02
N7343	22 36.6	33 59	4	6342	803	0.27
NGC 70	00 15.6	29 47	5	6402	614	0.04
NGC 83	00 18.6	22 12	7	5744	723	0.18
NGC 183	00 36.0	29 17	4	5222	102	0.14
NGC 295	00 52.2	31 20	5	5376	782	0.21
NGC 383	01 04.8	32 09	9	4808	461	0.08
NGC 403	01 06.6	32 17	5	4762	139	0.21
NGC 420	01 09.0	31 40	4	5047	313	0.23
NGC 507	01 19.8	33 04	23	4725	595	0.25
NGC 529	01 23.4	34 27	4	4608	247	0.08
A 262	01 50.4	36 11	18	4638	612	0.22
NGC 751	01 54.0	32 52	8	4616	376	0.10
A 347	02 22.2	41 47	5	5020	387	0.16
Perseus	03 15.6	41 19	19	5003	911	0.19

© American Astronomical Society • Provided by the NASA Astrophysics Data System

1993AJ....105.1251W

extensive group seen in the lower panel that defines the supercluster ridge. The panel immediately above shows the groups found at a density contrast of 30 000 times the mean density measured in the northern box. These groups contain the prominent Abell clusters, the Pisces cluster, and other dense peaks in the galaxian distribution. Those containing more than three members at the density contrast of 30 000 are listed in Table 3. The top panel shows the distribution of the 145 galaxies that are *not* found to be members of any group at a contrast of 20. No supercluster is evident in their sky distribution, although it should be noted that these objects still possess velocities which place them preferentially at the supercluster distance. They may be considered as outlining the outer layer of the supercluster enhancement.

4. EFFECTS OF ASPECT AND DISTANCE ON DETECTING NEARBY STRUCTURE

Here, we speculate on how the relative proximity of PP, our viewing angle, and its intrinsic high density linear concentration of galaxies, contribute to its appearance as one of the most conspicuous features of the extragalactic distribution of light.

4.1 Viewing Aspect and Orientation

It is evident from Figs. 1 and 4 that the supercluster ridge lies nearly in the plane of the sky. We may ask therefore how a changing perspective will affect the visibility of the supercluster structure. Figures 7(a)–7(d) illustrate

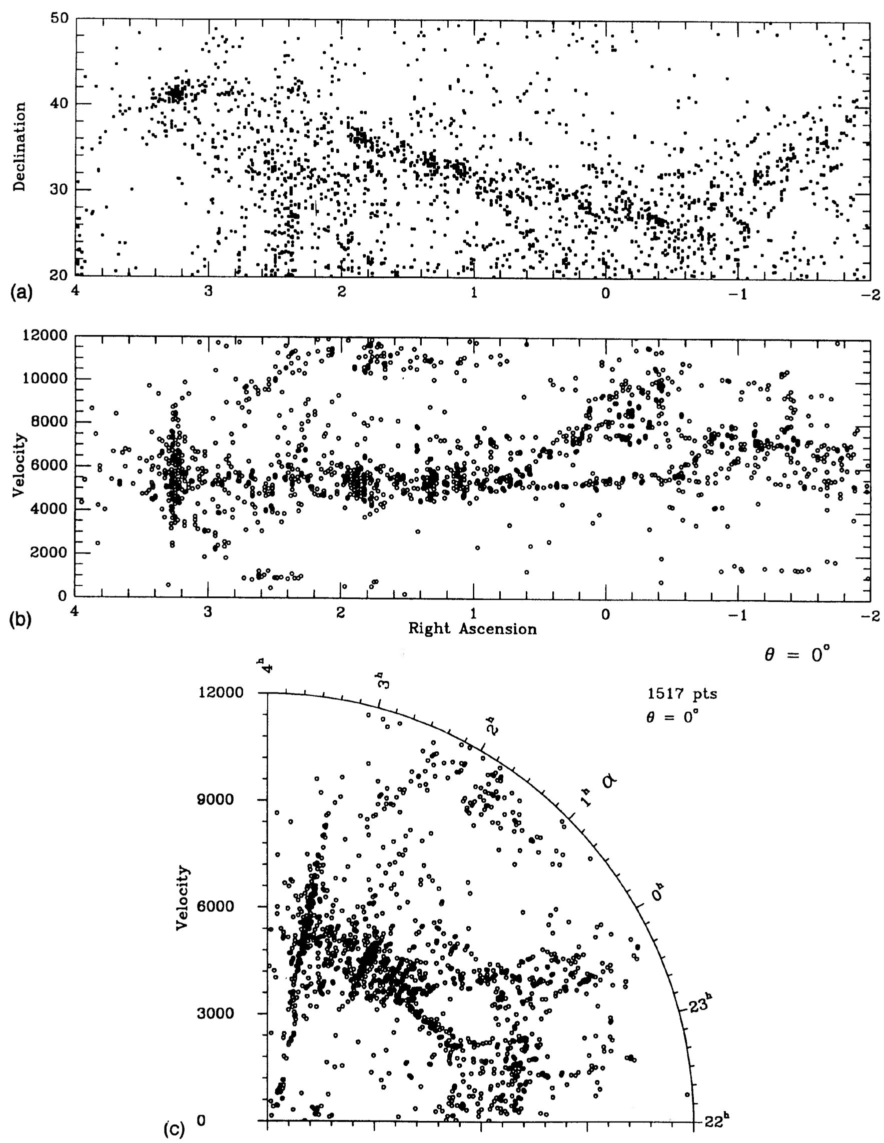

FIG. 7. The upper panels [(a),(b)] are the same two-dimensional slices as shown in Fig. 4, but now allowing for rotation of the linear supercluster ridge by an angle θ with respect to the plane of the sky. Here, $\theta=0°$. The bottom panel (c) shows the velocity cone diagram for all galaxies remaining in the apparent-magnitude limited sample. The rules of the rotation are described in the text. Only galaxies that remain in the apparent magnitude limited sample following rotation are included.

© American Astronomical Society • Provided by the NASA Astrophysics Data System

1993AJ....105.1251W

how varying the inclination of such a linear structure along the line of sight will affect its identification. In this simple treatment, we have rotated the supercluster in the R.A.–Velocity plane, by an angle θ with respect to the plane of the sky such that each galaxy's declination remains constant.

Rotation is performed so that the ridge is assumed to be a rigid, linear bar fixed at the eastern terminus, identified with the Perseus cluster. The ridge then rotates by θ with respect to the plane of the sky in the sense that increasing θ displaces the western (Pegasus) end of the supercluster away from us. We start from $\theta=0°$ (Fig. 7). Only galaxies found within the ridge region and having redshifts in the range 4500 km s$^{-1} < V_0 < 6500$ km s^{-1} are assumed to be in the supercluster. Galaxies in the ridge region with higher or lower velocities do not rotate. In addition, we artificially allow for a population of homogeneously distributed objects at the same distance by allowing ten percent of the supercluster galaxies to remain where they are, randomly chosen. If the galaxy meets the criterion for inclusion in the supercluster ridge and does not fall in the 10% "random" bin, then it moves with the rigid supercluster through its rotation. As θ and thus the distance to a given galaxy increase, three effects become evident: (1) its observed redshift increases; (2) its apparent separation from A426 decreases; and (3) it appears fainter. No differential galactic extinction corrections are applied, but the amount of fading due to increased distance is calculated and the object in its new location is tested for inclusion within an apparent magnitude cutoff of $m=15.7$.

The upper panels in Figs. 7–10 are similar in content to Fig. 1; only galaxies in the magnitude-limited samples with $V_0 < 12\,000$ km s^{-1} are shown, and the region of the ridge is not outlined in the upper panel. The lower cone diagram

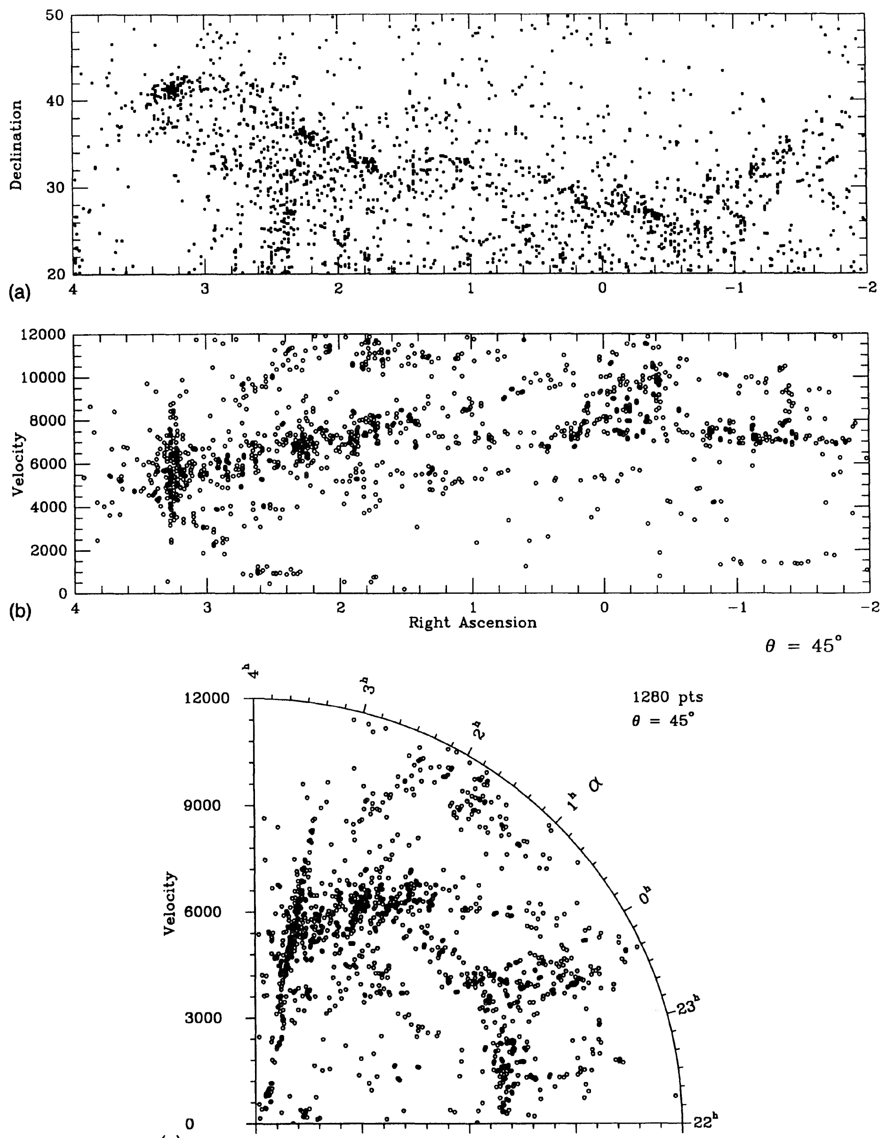

FIG. 8. Same as in Fig. 7, except that $\theta=45°$.

© American Astronomical Society • Provided by the NASA Astrophysics Data System

1993AJ....105.1251W

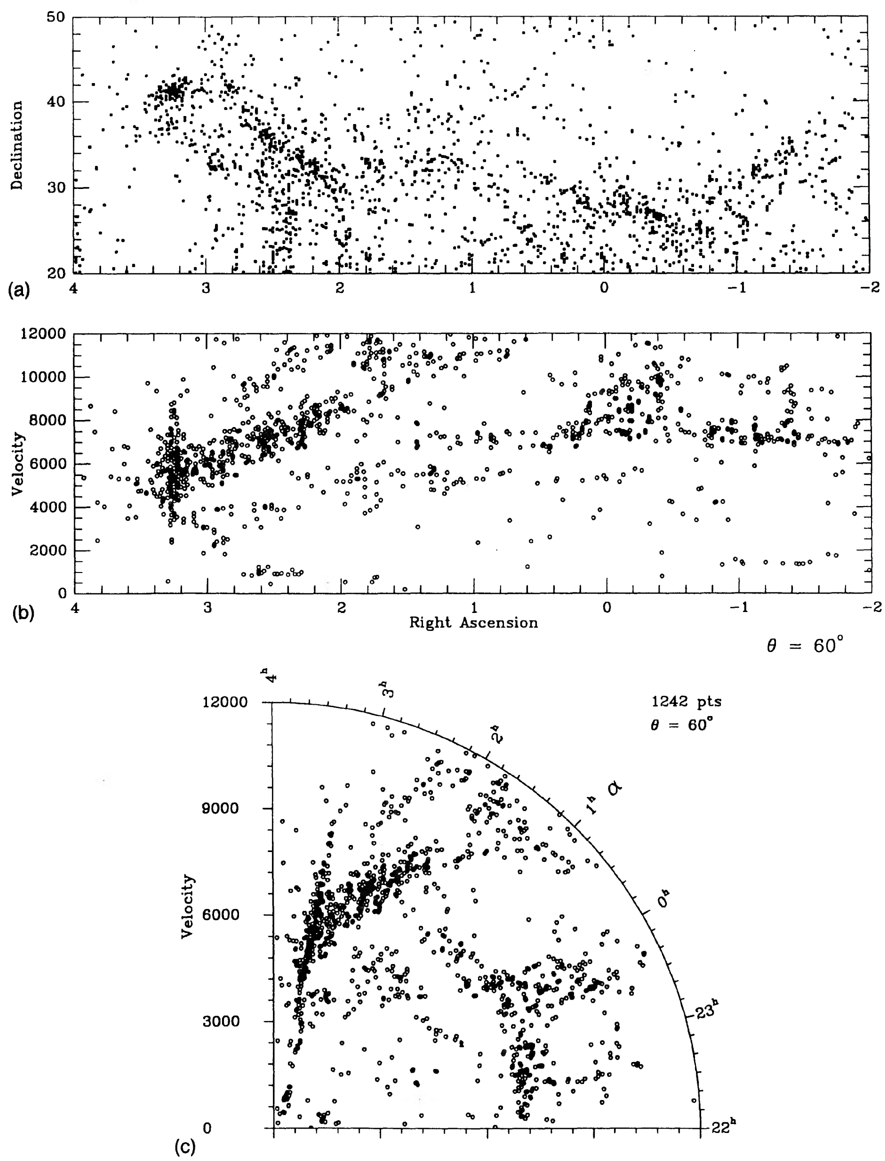

FIG. 9. Same as in Fig. 7, except that $\theta=60°$.

in each case shows the corresponding display for galaxies within the entire northern box and thus is to be compared with the upper cone diagram in Fig. 4. Also indicated is the number of objects that remain in the apparent magnitude limited sample after the rotation. For the $\theta=0°$ case, Fig. 7(a) shows the same features as Fig. 1 except that it contains only the galaxies with known redshift less than 12 000 km s^{-1} in the upper panel. The ridge is clearly evident and can be traced westward to the branching that occurs at R.A. $=0^h40^m$. The strong contrast relative to the foreground and background is most pronounced with the supercluster ridge oriented in the plane of the sky.

Figures 8–10 are identical to Fig. 7, but with rotation through the angle θ of 45°, 60°, and 75°, respectively. The ridge becomes increasingly harder to trace over large angular distances as the rotation angle increases; visual coherence is lost and the number of sampled galaxies that are part of the structure diminishes. The contrast of the supercluster ridge relative to its immediate foreground and background appears greatly reduced.

4.2 Distance Effects

In addition to its favorable orientation nearly in the plane of the sky, the PP ridge is also sufficiently close that large numbers of its galaxies are included in the UGC and CGCG catalogs and at the same time, far enough away that it subtends a relatively small angle in one dimension on the sky. As discussed by GHC, PP is at a convenient distance to be traced by catalogs like the UGC and CGCG because those catalogs sample galaxies fainter than the knee of the luminosity function at the supercluster's dis-

© American Astronomical Society • Provided by the NASA Astrophysics Data System

1993AJ....105.1251W

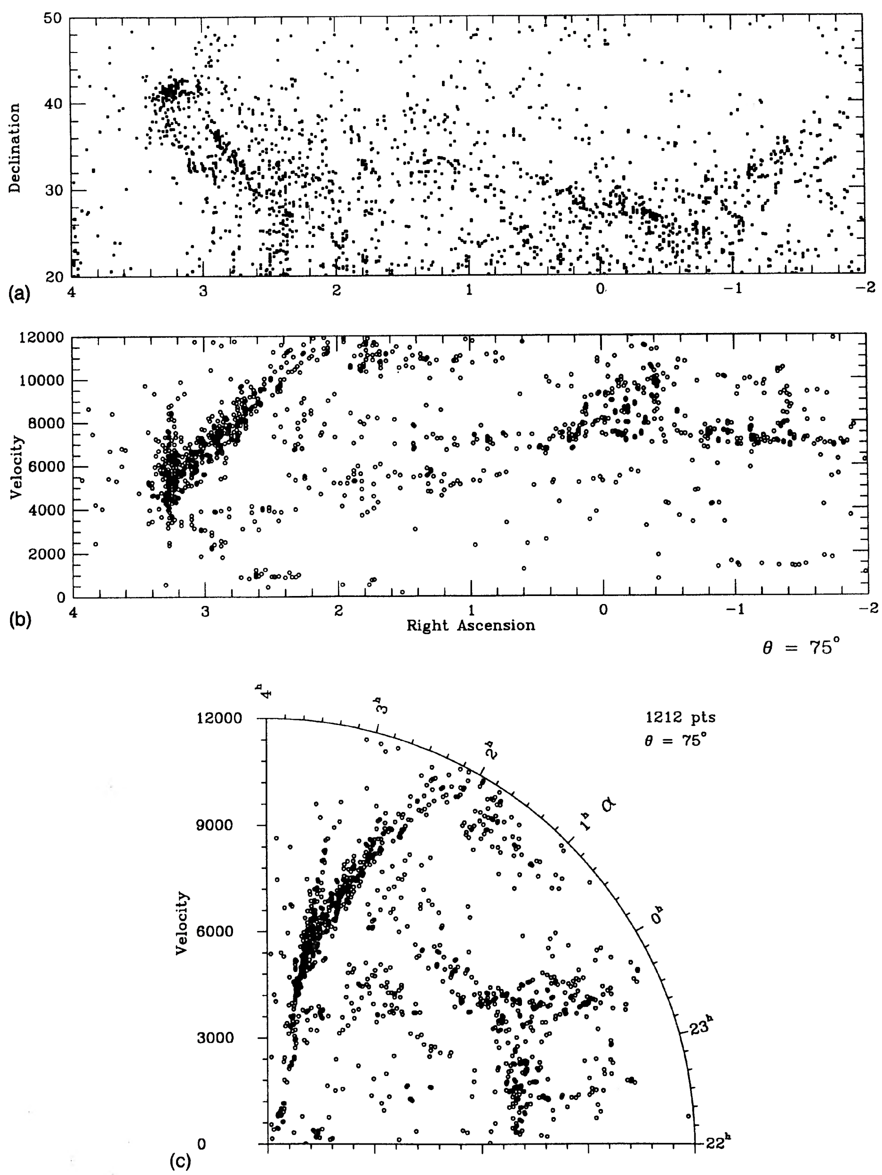

FIG. 10. Same as in Fig. 7, except that $\theta=75°$.

tance. As an example of the distance effect, we present in Fig. 11 how the supercluster ridge would appear if it were located instead at a redshift of 10 000 km s^{-1}. Similar to Fig. 7, Fig. 11 displays the two-dimensional representations for the case that the entire supercluster ridge is moved to that mean redshift. Each galaxy has its redshift increased by (10 000–5500) = 4500 km s^{-1}, the difference between the new mean redshift and that of A426. To serve as benchmarks, all galaxies found within two degrees of the Perseus cluster A426 (Kent & Sargent 1983) retain their original apparent magnitude; but for other objects, a new apparent magnitude is assigned according to the galaxy's intrinsic luminosity and its new distance. Each galaxy is tested again for inclusion in the apparent magnitude limited sample. As before, only objects believed to be in the PP ridge are moved and ten percent of them are randomly allowed to remain at their current locations.

The analog of A426 now is located at a redshift of 10 000 km s^{-1}. A comparison of the uppermost panel with that in Fig. 7(a) shows a great reduction in the sampling of the other clusters. Some structure at 5000 km s^{-1} remains in the cone diagram, contributed by the more dispersed supercluster population found in the northern box but not within the ridge itself. A feature like PP found twice as far away would still be noticeable in redshift surveys, but it would also be quite inconspicuous in sky projection.

5. SUMMARY AND CONCLUSIONS

In this paper, we have presented new observational results in the form of optical redshifts and 21 cm line emission profiles for, respectively, 229 and 315 galaxies, in the volume that includes the main ridge of the PP supercluster. In addition to presenting the observations, the purpose of

© American Astronomical Society • Provided by the NASA Astrophysics Data System

1993AJ....105.1251W

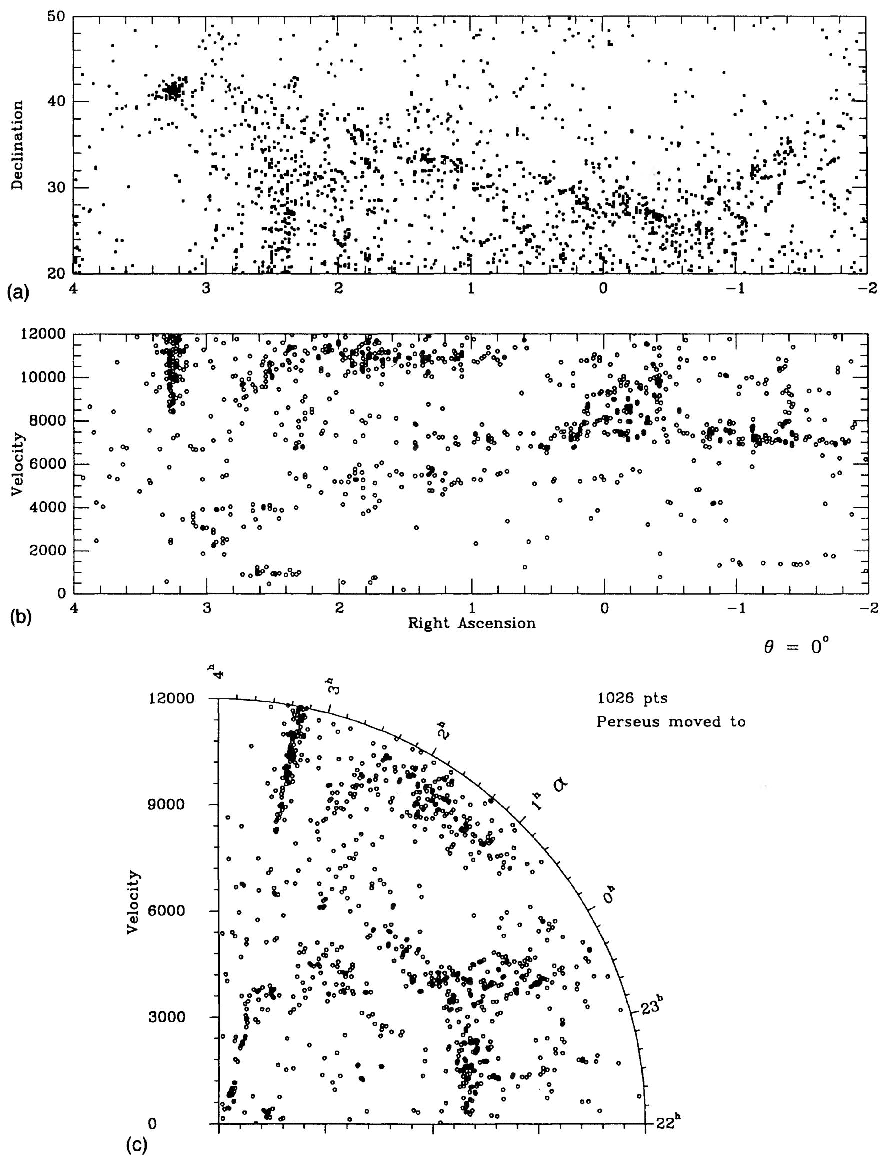

FIG. 11. Same as in Fig. 7 but for a supercluster ridge like PP located twice as far away.

the current paper is to give the reader a rough impression of the supercluster geometry, the linearity of its structure, its overdensity, and the unique aspects that make it such a favorable target for the study of large-scale structure in the local universe. We can summarize the main characteristics of the PP supercluster as evidenced by the data available today as follows.

(1) The main ridge of the supercluster extends at least $50h^{-1}$ Mpc from Pegasus eastward to the Perseus cluster, where it then disappears into the Zone of Avoidance. There are suggestions that its continuity is maintained behind the galactic plane (Giovanelli & Haynes 1982), but statistics tracing the extension are still poor.

(2) The width of the ridge in the plane of the sky is about 5–$10h^{-1}$ Mpc. The main ridge lies roughly at the same distance from us at all points along its length.

(3) In comparison with what is expected for a randomly-distributed, well-behaved population, the redshift distribution (Figs. 1 and 4) reveals a significant overdensity at 5000 km s^{-1} and a prominent underdensity in the foreground. This void is seen over the entire PP survey region.

(4) Typical depths in redshift are of order 250–500 km s^{-1} with occasional velocity spreading due to the presence of clusters. Locally, and after the removal of mild velocity gradients, features of even lower velocity dispersion are seen, notably between R.A. $=23^h40^m$ and 00^h15^m.

(5) A continuous arrangement of high density clusters and groups is seen in the PP ridge. The ridge is best defined by the highest density subconcentrations around the Pisces clusters, Abell 262 and Abell 426.

(6) The relative proximity, high density contrast, and

© American Astronomical Society • Provided by the NASA Astrophysics Data System

1993AJ....105.1251W

favorable orientation of the linear ridge structure give it high visibility in both sky projection and velocity-cone diagrams. Similar structures viewed more aligned with the line of sight or at twice the distance would be much harder to recognize.

(7) The PP supercluster dominates the structure seen in the anti-Virgo direction. Not only is there a foreground void separating PP from the Local Supercluster, but an underdensity also exists over much of its length in the background at a recessional velocity of $\simeq 8000$ km s^{-1}. The presence of such large-scale density inhomogeneities make it difficult to use portions of this volume to measure a fair value of the mean density.

This work has been partially supported by NSF Grant Nos. AST-9017048 to G.W. AST-9023450 to M.P.H. and AST-9115459 to R.G.

We would like to thank Miguel Boggiano, José Cruz, Norberto Despiau, Willy Portalatin, Ernesto Ruiz, Benjamin Santiago, Willy Torres, Angel Vázquez, and Rey Vélez for providing a competent and stimulating environment for observations at Arecibo, for often carrying out observations *in absentia* and, most importantly, for their dedication and good humor. Finally, we would like to thank Fred. S. Arena for providing a stimulating environment for discussions.

REFERENCES

Abell, G. O. 1958, ApJS, 3, 211
Bernheimer, W. E. 1932, Nature, 130, 132
Dressel, L. L., & Condon, J. J. 1976, ApJS, 31, 187
Eder, J. A., Schombert, J. M., Dekel, A., & Oemler, Jr., A. 1989, ApJ, 340, 29
Einasto, J., Joeveer, M., & Saar, E. 1980, MNRAS, 193, 353
Freudling, W. 1990, Ph.D. thesis, Cornell University
Giovanelli, R., & Haynes, M. P. 1982, AJ, 87, 1355
Giovanelli, R., & Haynes, M. P. 1985, AJ, 90, 2445
Giovanelli, R., & Haynes, M. P. 1989, AJ, 97, 633
Giovanelli, R., & Haynes, M. P. 1991, ARA&A, 29, 499
Giovanelli, R., Haynes, M. P., & Chincarini, G. L. 1986, ApJ, 300, 77 (GHC)
Giovanelli, R., Haynes, M. P., Myers, S. T., & Roth, J. 1986, AJ, 92, 250
Gourgoulhon, E., Chamaraux, P., & Fouqué, P. 1992, A&A, 225, 69
Gregory, S. A., Thompson, L. A., & Tifft, W. G. 1981, ApJ, 243, 411
Haynes, M. P., & Giovanelli, R. 1984, AJ, 89, 758 (HG84)
Haynes, M. P., & Giovanelli, R. 1986, ApJ, 306, L55
Haynes, M. P., & Giovanelli, R. 1988, in Large-Scale Motions in the Universe, edited by V. C. Rubin and G. F. Coyne (Princeton University Press, Princeton), p. 45
Haynes, M. P., & Giovanelli, R. 1991, AJ, 102, 841
Haynes, M. P., Giovanelli, R., Starosta, B., & Magri, C. A. 1988, AJ, 95, 607
Hewitt, J. N., Haynes, M. P., & Giovanelli, R. 1983, AJ, 88, 272
Huchtmeier, W. K., & Richter O.-G. 1989, A General Catalog of H I Observations of Galaxies (Springer, New York)
Huchra, J. P., & Geller, M. J. 1982, ApJ, 257, 423
Kent, S. M., & Sargent, W. L. W. 1983, AJ, 88, 697
Magri, C. A. 1990, Ph.D. thesis, Cornell University
Nilson, P. 1973, in Uppsala General Catalog, Uppsala Astron. Obs. Ann. 6 (UGC)
Sakai, S., Giovanelli, R., & Wegner, G. A. 1993, in preparation
Sandage, A. 1961, The Hubble Atlas of Galaxies (Carnegie Institution of Washington, Washington)
Sandage, A., & Tammann, G. A. 1987, A Revised Shapley–Ames Catalog of Bright Galaxies (Carnegie Institution, Washington)
Sargent, W. L. W., Schechter, P. L., Boksenberg, A., & Shortridge, K. 1977, ApJ, 212, 326
Struble, M. F., & Rood, H. J. 1987, ApJS, 63, 555
Tody, D. 1986, Proc. SPIE, 627, 733
Zwicky, F., Herzog, E., Karpowicz, M., Kowal, C. T., & Wild, P. 1961–1968, Catalogue of Galaxies and Clusters of Galaxies (California Institute of Technology, Pasadena), Vols. 1–6 (CGCG)

© American Astronomical Society • Provided by the NASA Astrophysics Data System